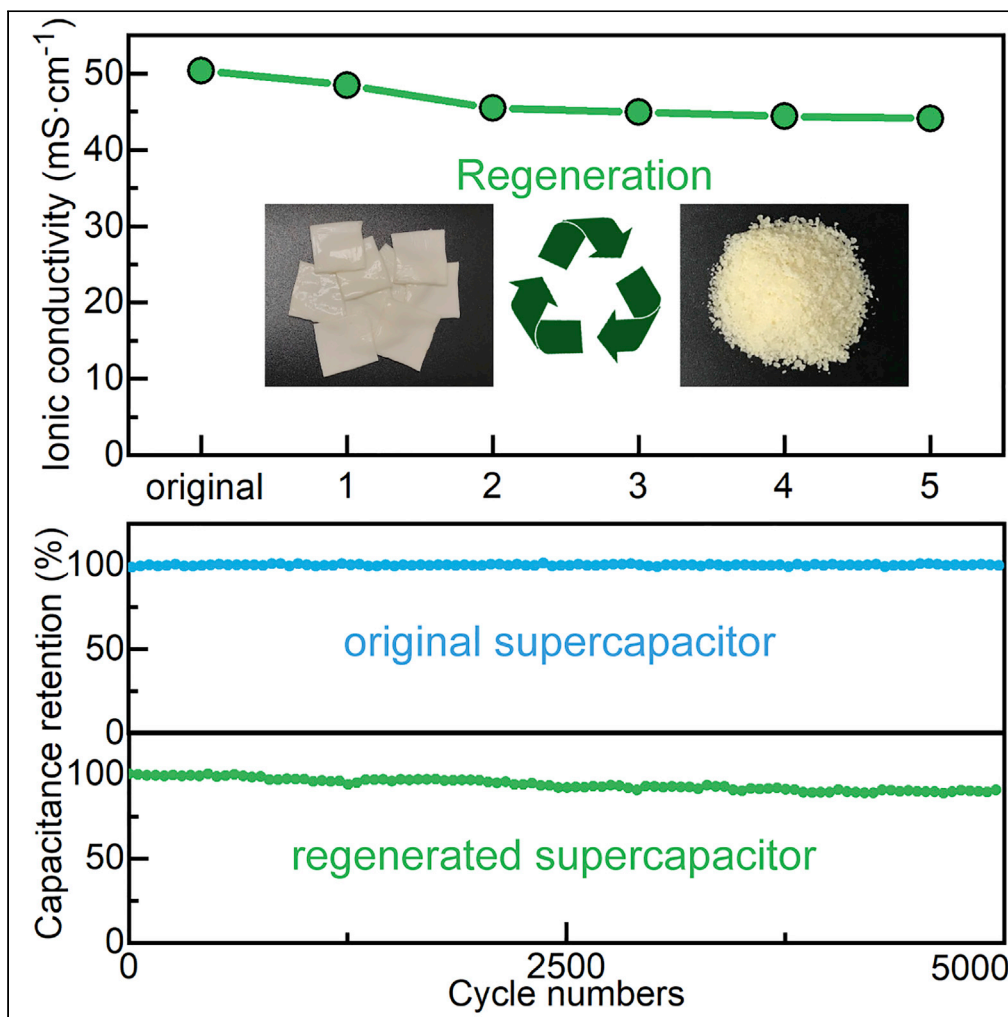


## Article

## A Regenerable Hydrogel Electrolyte for Flexible Supercapacitors



Guanbing Zhou,  
Leyi Yang, Weijun  
Li, Chongyi Chen,  
Qiao Liu

chenchongyi@nbut.edu.cn  
(C.C.)  
liuqiao@nbut.edu.cn (Q.L.)

**HIGHLIGHTS**  
Highly reliable PAA-PAH/  
LiCl electrolyte for flexible  
supercapacitor is  
developed

PAA-PAH/LiCl hydrogel  
electrolyte can be easily  
regenerated under mild  
conditions

Regenerated hydrogel  
shows high retention of  
ionic conductivity and  
extensibility

Regenerated device  
reserves >90%  
capacitance and durability  
of the original one

Zhou et al., iScience 23,  
101502  
September 25, 2020 © 2020  
The Authors.  
<https://doi.org/10.1016/j.isci.2020.101502>



## Article

# A Regenerable Hydrogel Electrolyte for Flexible Supercapacitors

Guanbing Zhou,<sup>1</sup> Leyi Yang,<sup>1</sup> Weijun Li,<sup>1</sup> Chongyi Chen,<sup>1,3,\*</sup> and Qiao Liu<sup>2,\*</sup>

## SUMMARY

**Easy regenerability of core components such as electrode and electrolyte is highly required in advanced electrochemical devices. This work reports a reliable, regenerable, and stretchable hydrogel electrolyte based on ionic bonds between polyacrylic acid (PAA) and polyallylamine (PAH). PAA-PAH electrolyte (1M LiCl addition) exhibits high ionic conductivity (0.050 S·cm<sup>-1</sup>) and excellent mechanical property (fracture strain of 1,688%). Notably, the electrolyte can be regenerated to any desired shape under mild conditions and remains 96% and 90% of the initial ionic conductivity after the first and second regeneration, respectively. PAA-PAH/LiCl-based supercapacitor exhibits nearly 100% capacitance retention upon rolling, stretching, and 5,000 charge-discharge cycles, whereas the regenerated device holds 97.6% capacitance of the initial device and 90.9% after 5,000 cycles. This low-cost, high-efficiency, and regenerable hydrogel electrolyte reveals very promising use in solid-state/flexible supercapacitors and possibly becomes a standard commercial hydrogel electrolyte for sustainable electrochemical energy devices.**

## INTRODUCTION

The growing development of wearable electronics has triggered the emerging demand for modern energy storage/conversion systems, which calls for the whole device to maintain the excellent electrochemical performance under various mechanical strains (Wang et al., 2018c; Pomerantseva et al., 2019; Ray et al., 2019). Flexible supercapacitors (SCs), as a typical representative, are drawing intense attention owing to their high power density and long cycle life (Lu et al., 2013; Niu et al., 2013; Wang et al., 2014b, 2015; Liu et al., 2017; Ren et al., 2018; Chen et al., 2019a). Yet as subjected to practical applications, these SCs may suffer from structural damage caused by overtime deformation or severe mechanical impact, eventually leading to the device malfunction, additional energy cost, and abundant wastes as well (Hu et al., 2010; Li et al., 2015; Oh et al., 2016). The improvement of reliability and lifetime has become a key issue to realize ideal wearable SCs, whereas most of the current research on flexible SCs has focused on fabricating novel electrode materials with enhanced capacitances or minimized dimensions for easy compatibility with various device architectures (Cai et al., 2016; Huang et al., 2016; Xue et al., 2017; Kumar et al., 2018). Recently, the quasi-solid polymer electrolyte, another core component of flexible SCs usually fulfilling dual roles of electrolyte and separator, are receiving increasing research interest in portable, wearable SCs owing to their high ionic conductivity and low risk of electrolyte leakage, such as hydrogel electrolytes (Song et al., 2019; Park et al., 2020; Wang et al., 2020).

Till now, polyvinyl alcohol (PVA) is the most widely used electrolyte among the polyelectrolytes-based flexible SCs ever reported, because it is non-toxic, low in cost, and simple to process (Hu et al., 2017; Wang et al., 2018b). But there are some inherent shortcomings of PVA that have severely limited its widespread use. First, the dissolution of PVA powder in water requires the assistance of high temperature, and a general addition of strong acid/basic such as H<sub>2</sub>SO<sub>4</sub> or NaOH is demanded to improve ionic conductivity of PVA aqueous solution, both of which allow easy oxidization of PVA and contribute to an unstable electrochemical performance. Second, the PVA electrolyte (generally used as a mixture of PVA/salt/water) with disordered physical cross-links shows a thick liquid form rather than a fixed shape (Peng et al., 2018). This means a flexibility dependence of the electronic device on the electrodes and even substrates, which demands the extra use of separator and flexible substrates (Lv et al., 2019), and even worse, increases the difficulty in maintaining structural integrity of the whole device and device's capacitance at high strains as well. Even though PVA can be modified to realize quasi-solid gels by

<sup>1</sup>State Key Laboratory Base of Novel Functional Materials and Preparation Science, School of Materials Science and Chemical Engineering, Ningbo University, Ningbo 315211, China

<sup>2</sup>Institute of Materials, Ningbo University of Technology, Ningbo 315016, China

<sup>3</sup>Lead Contact

\*Correspondence:  
chenchongyi@nbu.edu.cn  
(C.C.),  
liuqiao@nbu.edu.cn (Q.L.)

<https://doi.org/10.1016/j.isci.2020.101502>



hydrogen bonds (Yang et al., 2020), it still suffers from the low water uptake and retention, which not only puts strict requirements on operating temperature and packaging technology of the device but also leads to a significant reduction in ionic conductivity and cycling stability of resultant SCs (Su et al., 2016). Also, these modified PVA gels often exhibit unsatisfactory flexibility and mechanical strength, which generally varies with the types of PVA and specific preparation methods (Zhang et al., 2015). Last but not the least, PVA is difficult to regenerate, manifesting high energy cost accompanied with severe environmental pollution from strong acid/basic chemicals added (Meng et al., 2010; Lu et al., 2014). Self-healing and even regenerability is one of the most effective approaches to resolve the practical performance deterioration of flexible electronic devices caused by inevitable physical damage of polymer electrolyte. As for aforementioned limitations, therefore, it is highly desirable to develop low-cost and reliable PVA alternatives that are soft, durable, and regenerable to accommodate long-standing movements of flexible SCs devices in practical use.

Recently, some new hydrogel electrolytes for SCs have been exploited for their feasibility to design and fabricate unprecedented energy storage devices with additional functions, to name a few, a zwitterionic gel of propylsulfonate dimethylammonium propylmethacrylamide demonstrating robust water retention ability and excellent rate capacity (Peng et al., 2016), vinyl hybrid silica nanoparticle cross-linked polyacrylamide (PAAm) electrolyte with super-stretchability/compressibility and good ionic conductivity (ca. 17 mS cm<sup>-1</sup>) (Huang et al., 2017), a double cross-linked hydrogel based on covalently cross-linked PAAm and Al<sup>3+</sup> cross-linked alginate that shows super toughness and high ionic conductivity (ca. 29 mS cm<sup>-1</sup>) (Liu et al., 2019b), cross-linked dopamine-grafted alginate/KCl hydrogel electrolyte for self-healable and cold-resistant SCs (Tao et al., 2017), and a dynamic PVA-based network cross-linked by diol-borate ester bonding showing great capacitive restoration after breaking/healing cycles (Wang et al., 2016). What's more, most of them can self-heal when slightly damaged, as for serious damage and even fragmentation, regenerability that has much better self-healing ability is required (the difference between self-healing and regeneration process is shown in Figure S1) (Qu et al., 2019). The current research comprises striking omissions in the regenerability and structural sustainability of hydrogel electrolytes for solid-state SCs regenerated at the device level, which poses a huge challenge for the low-cost fabrication of highly reliable solid-state/flexible SCs toward enhanced practicability.

In order to introduce great regenerability into the hydrogel electrolyte, high density of non-covalent bonds between polymers is highly demanded. In this regard, a polyelectrolyte hydrogel based on commercialized low-cost polymer materials was developed in this study, comprising polyacrylic acid (PAA) and polyallylamine (PAH), two oppositely charged polyelectrolytes. As-formed high density of ionic bonds along the polymer backbone could endow the hydrogel with great regenerability; on the other hand, the high density of ionic bonds between PAA and PAH can significantly enhance the mechanical property of hydrogel. The ionic bonded PAA and PAH hydrogel electrolyte mixing with 1.0 M LiCl (PAA-PAH/LiCl) that demonstrates great ionic conductivity (0.050 S·cm<sup>-1</sup>), excellent mechanical properties (strain at fracture of 1,688%, stress at fracture of 57.0 kPa) and regenerability (96% and 90% of the original ionic conductivity after the first and second regeneration, respectively). SCs based on this gel electrolyte deliver an ultrahigh cycling stability (nearly 100% capacitance retention after 5,000 charge-discharge cycles), great flexibility (nearly 100% capacitance retention at the crimping and stretching states), and excellent regenerability (97.6% capacitance retention for the completely regenerated device), demonstrating great promise as a practical electrolyte for uses in durable, flexible, regenerable SCs.

## RESULTS

Figure 1A illustrates the typical straightforward one-pot synthesis of PAA-PAH/LiCl hydrogel electrolyte without complex multiple-step preparation of hydrogel and further immersion of hydrogel in salt aqueous solution, which shows great universality and convenience. As-prepared PAA-PAH hydrogel is cross-linked by ionic bonds between poly (ammonium) and poly (carboxylate). It can be evidenced by Fourier transform infrared (FTIR) spectroscopy (Figure S2), where the signals at 1,565 and 2,848 cm<sup>-1</sup> correspond to the characteristic adsorption for COO<sup>-</sup> (PAA) and NH<sub>3</sub><sup>+</sup> (PAH), respectively (Yuan et al., 2019b). Tensile test was performed to reveal mechanical features of as-prepared hydrogel electrolyte. As shown in Figure 1B, it is of excellent mechanical property with strain at fracture of 1,688% and stress at fracture of 57.0 kPa. In addition, it can be easily stretched to a high strain without any visible crack (Figure S3). The excellent extensibility can be attributed to the rapid recovery of ionic bonds.

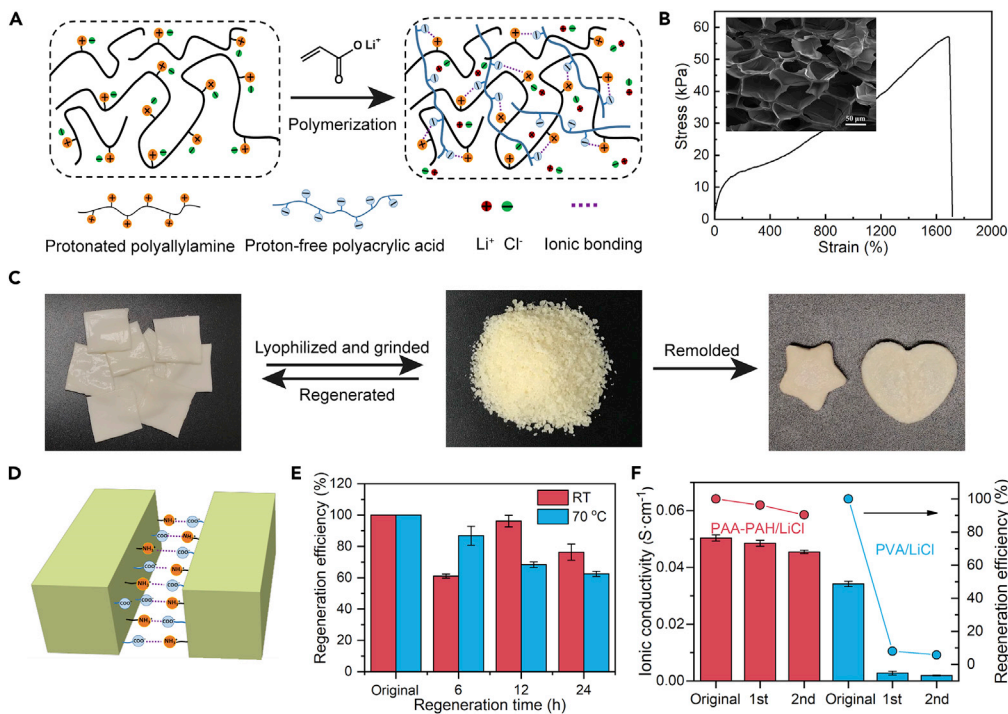


**Figure 1. Preparation Process and Regeneration Property of Hydrogel Electrolyte**

- (A) Schematic illustration of the preparation of PAA-PAH/LiCl hydrogel electrolyte.
- (B) Stress-strain curve of PAA-PAH/LiCl. Inset: SEM image of PAA-PAH/LiCl.
- (C) The regeneration and remolding of PAA-PAH/LiCl.
- (D) The regeneration mechanism of PAA-PAH/LiCl.
- (E) The regeneration efficiency under different temperatures calculated according to the ratio of the ionic conductivity of the regenerated PAA-PAH/LiCl to the original one. Error bars represent standard deviations from three independent measurements.
- (F) The ionic conductivity of the original and regenerated (first and second) PAA-PAH/LiCl and PVA/LiCl hydrogel electrolytes. Error bars represent standard deviations from three independent measurements.

The ionic conductivity of the PAA-PAH/LiCl gel electrolyte with the extra addition of 1 M LiCl was tested to be  $0.050 \text{ S}\cdot\text{cm}^{-1}$ , manifesting a high level among hydrogel electrolytes ever reported (Table S1 and Figure S4). In particular, this PAA-PAH/LiCl gel electrolyte holds higher ionic conductivity than most of PVA gel-based electrolytes (Wang et al., 2016; Geng et al., 2019; Huang et al., 2019; Peng et al., 2019; Sun et al., 2019; Zhou et al., 2019; Liu et al., 2020; Lu and Chen, 2020; Lu et al., 2020) with the same amount of salt addition. This indicates a greater application prospect of PAA-PAH/LiCl than PVA-based gel electrolytes. At the same time, its ionic conductivity is comparable with and even greater than most of modified PAA and PAM-based gel electrolytes (e.g., gelatin-g-PAAm [Li et al., 2018], PAA-co-PAAm [Dai et al., 2019], agar/PAAm [Fang et al., 2019], alginate/PAAm [Liu et al., 2019b] and Li-agar/PAAm [Lin et al., 2018]) and other gel electrolytes (e.g., poly(vinylimidazole-hydroxypropyl acrylate) [Wang et al., 2017], Li-alginate [Ye et al., 2018] and chitosan-alginate [Zhao et al., 2018]) with same level of salt addition. Considering its unique molecular structure, the high ionic conductivity is inferred to occur in a synergistic manner: (1) easy separation of the cationic and anionic counter ions within this polyelectrolyte gel electrolyte during ion migration process (Peng et al., 2016; Lee et al., 2018); (2) large amounts of carboxylate and ammonium on polymer chains enabling a high electrolyte adsorption capacity and thus a high ion conductivity of the gel electrolyte; (3) 3D porous network structure of PAA-PAH/LiCl (Figure 1B inset) that facilitates ion transport, further ensuring a high ionic conductivity (Guo et al., 2016).

Benefiting from the multiple reversible physical cross-links between molecular chains, PAA-PAH/LiCl gel electrolyte is expected to possess eminent regenerability. In order to study the regenerability and explore its easy processability, PAA-PAH/LiCl hydrogel was regenerated as the following procedures (Figure 1C): first, hydrogel was lyophilized (the pristine water content was ca. 60.7%) and grinded into hundreds-

micrometer fine powder; second, the cryogel powder was then placed in a mold with equal ratio of water addition and sealed by a glass plate with a small pressure to ensure the close contact between powders. Regenerated hydrogel of any desired shapes can be obtained ([Figure S5](#)), suggesting the possible use in constructing devices with customized structures to fit various application needs. The regeneration process of PAA-PAH/LiCl was investigated via a 3D microscope ([Figure S6](#)). First, the cryogel powders were immersed in water; after 12 h, the particles swelled by absorbing water and fused together accompanying with the disappearance of micrometer-scale voids in bulk material; after another 12 h, further swelling resulted in the disappearance of millimeter-scale cracks; meanwhile, the porous structure was regenerated and filled with electrolyte solution. The regenerability of PAA-PAH/LiCl can be ascribed to the high density of anion/cation groups along polymer chains that can form dynamic ionic bonds driving the rapid regeneration of hydrogel in the presence of water ([Luo et al., 2015](#); [Yuan et al., 2019a](#)), as illustrated in [Figure 1D](#).

To determine the optimal regenerating conditions, the hydrogel electrolyte was regenerated at varied duration from 6 to 24 h and different temperatures from room temperature (RT) to 70°C. The regeneration efficiency calculated in this work was the ratio of the ion conductivity of the regenerated sample to the original one for evaluating the viability of future applications in electrochemical devices. As shown in [Figure 1E](#), at RT, the regeneration efficiency of the sample increases with the elongation of regeneration time until 12 h, reaching a maximum of 96%. The regeneration efficiency at a higher temperature of 70°C behaves differently, where the optimal regeneration time occurs at 6 h, and then the ion conductivity of regenerated samples declines with longer time. Considering the demands of sufficient water absorption and the repair of countless wound surfaces, high temperature and long time are favorable for the full “bonding” of cryogel powders. Yet with the time extension, the drop of regeneration efficiency occurs at both temperatures, and instead, the lower temperature of RT causes higher value of ionic conductivity at 12 and 24 h. In that case, the other side of high temperature and long time need to be considered, both of which are detrimental to the retention of moisture in the gel electrolyte. Given our mold was not 100% sealed, the decreased water content as the increase of regenerating time and temperature could result in the reduced regeneration efficiency. Under the current experimental conditions, therefore, the optimal and cost-effective regeneration condition is 12 h at room temperature.

It is worth mentioning that this is the first report investigating ionic conductivity of the regenerated hydrogel electrolyte. To explore its practicability, PVA, the most widely used hydrogel electrolyte at present, was tested as comparison. PVA/LiCl hydrogel was prepared by the freeze-thaw procedure adopted in many reports ([Guo et al., 2018](#); [Hu et al., 2018](#)), with the water content of ~75.6% and an original ionic conductivity of 0.034 S·cm<sup>-1</sup>. Then, through identical regeneration procedure with PAA-PAH/LiCl, PVA/LiCl hydrogel shows sharp decline of ionic conductivity to 0.003 and 0.002 S·cm<sup>-1</sup> after the first and second regenerations, respectively ([Figure 1F](#)). In contrast, the ionic conductivity of PAA-PAH/LiCl hydrogel electrolyte was estimated to be 0.048 and 0.045 S·cm<sup>-1</sup> after the first and second regenerations, i.e., 96% and 90% retention of the initial value (0.050 S·cm<sup>-1</sup>), respectively. In addition, the ionic conductivity of PAA-PAH/LiCl can retain 0.044 S·cm<sup>-1</sup> even after the fifth regeneration ([Figure S7](#)). The excellent regenerability can also be confirmed by mechanical test, where PAA-PAH/LiCl retains 88% and 85% of original fractural strain after the first and fifth regenerations, respectively ([Figure S8](#)). The slight decrease of ionic conductivity and fractural strain after multiple regenerations can be attributed to the partial irreversible fracture of polymer backbones (C-C covalent bonds) during the grinding of cryogel, resulting in the irreversible impairment of polymeric network structure. Regarding the high ionic conductivity and excellent regenerability, PAA-PAH/LiCl demonstrates to be a versatile hydrogel electrolyte deserving more practical use in solid-state and flexible energy storage/conversion devices than PVA/LiCl. Meanwhile, the good regenerability together with easy processing also makes it to be an ideal commercial option that can be put into industrial production. In order to explore its practical use in solid-state/flexible SCs with regenerability, PAA-PAH/LiCl-based SCs were assembled by sandwiching two pieces of PANI@CNTs electrodes with a PAA-PAH/LiCl layer ([Figure S9](#)), where PANI acts as the capacitance active species and CNT paper provides flexible support and increases the electrical conductivity of active PANI material ([Eftekhari et al., 2017](#)).

A series of PANI@CNTs electrodes was prepared by varying the electrochemical deposition time of PANI from 0 to 15 min. Observed from SEM images of corresponding samples ([Figure S10](#)), different deposition times share a similar PANI-nanowires morphology from top view. The difference lies in the thickness of PANI layer anchored on CNTs paper, which can be certified by the estimation of the areal loading amounts varied by deposition time, i.e., 0.13, 0.40, 1.27, 1.73, 2.33, 3.33 mg cm<sup>-2</sup> at 1.0, 2.5, 5.0, 7.5, 10, 15 min,

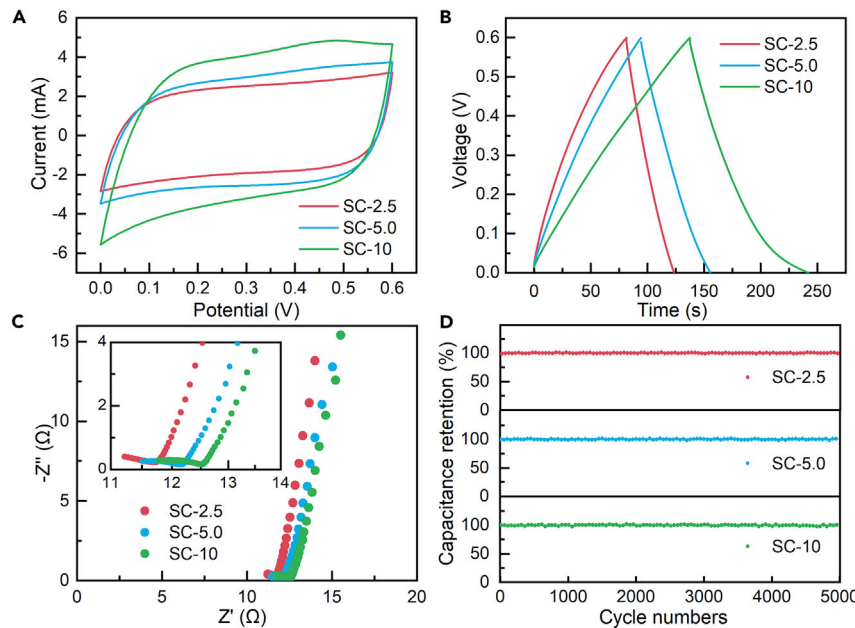


**Figure 2. Electrochemical Characterization of As-assembled Solid-State Supercapacitors**

(A) CV curves of SC-2.5, SC-5.0, and SC-10 at a scan rate of 50 mV s<sup>-1</sup>.

(B) GCD curves of SC-2.5, SC-5.0, and SC-10 at a charge-discharge current density of 0.2 mA cm<sup>-2</sup>.

(C) Nyquist plots of SC-2.5, SC-5.0, and SC-10. Inset: magnified Nyquist plots.

(D) Cycling performance of SC-2.5, SC-5.0, and SC-10 for 5,000 cycles.

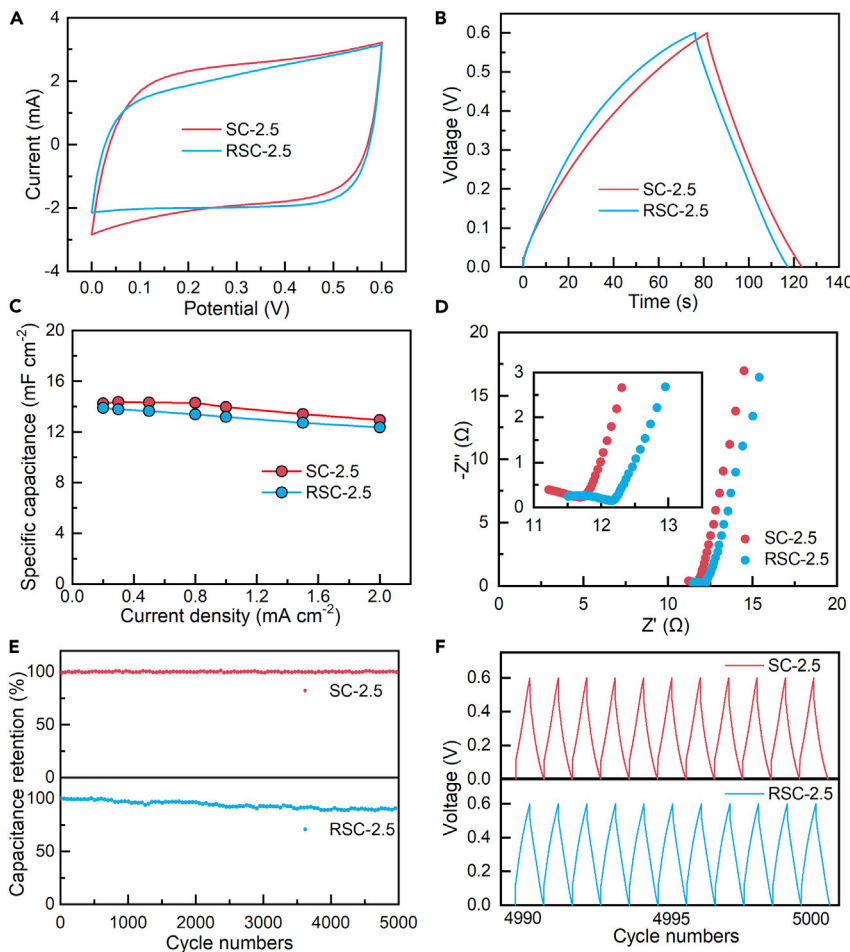
respectively. Then, the influence of deposition time on the specific capacitance ( $C_s$ ) of the PANI@CNTs electrode was examined in a typical three-electrode system.  $C_s$  figures of all PANI@CNTs electrodes were calculated according to galvanostatic charge-discharge (GCD) curves in different discharge currents, as shown in Figure S11. It is easy to find that the mass specific capacitance ( $C_m$ ) of the PANI@CNTs electrode decreases as its deposition time increases, where the maximum of 2,465 F g<sup>-1</sup> (1 mA cm<sup>-2</sup>) occurs at 1 min of deposition, indicating the optimal utilization of active sites corresponded to the least active material per unit area. As for area specific capacitance ( $C_a$ ), another important parameter to evaluate film electrodes used in flexible or microscopic SCs, it keeps increasing as extending PANI deposition time to 10 min, reaching the maximum of 630 mF cm<sup>-2</sup> (1 mA cm<sup>-2</sup>), and then a slight decline occurs at 15 min of deposition. So, upon the increase of deposition time, the resultant increased amount of active material makes for an improved capacitance of electrodes, but the denser and thicker structure of PANI layer simultaneously puts more stress on the smooth charge/mass transfer, thereby leading to the reduction of charge capacitance and poor rate performance as well. Excessive active material, on the other hand, is difficult to closely adhere on the electrode surface especially in practical use with repetitive deformations, so the easily detached part of active material would inevitably result in a poor reliability of the electrode and even the whole device. Taken together, the optimum deposition time of PANI should be determined according to the specific use environments, normally no more than 10 min.

Subsequently, a series of SCs based on PAA-PAH/LiCl hydrogel electrolyte and PANI@CNTs electrodes deposited for 2.5, 5.0, and 10 min were assembled and tested, and for convenience, they were named SC-2.5, SC-5.0, and SC-10, respectively. Figure 2A displays cyclic voltammetry (CV) curves of above three devices at a scan rate of 50 mV s<sup>-1</sup>, where both SC-2.5 and SC-5.0 display more symmetrical quasi-rectangular shape than SC-10, indicating a highly reversible energy storage process in low-loaded devices and also the low diffusion resistance due to the excellent conductivity of PAA-PAH/LiCl electrolyte. Accordingly, the  $C_m$  values of SC-2.5, SC-5.0, and SC-10 were calculated to be 16.23 (6.60 mF cm<sup>-2</sup>), 7.90 (8.09 mF cm<sup>-2</sup>), and 6.17 F g<sup>-1</sup> (10.49 mF cm<sup>-2</sup>) at a high scan rate of 50 mV s<sup>-1</sup>. The  $C_m$  decrease with the increase in PANI loading is accordance with the result in three-electrode system. According to the GCD curves collected at a discharge current density of 0.2 mA cm<sup>-2</sup> (Figure 2B), as-calculated  $C_m$  values of SC-2.5, SC-5.0, and SC-10 are 17.51 (14.24 mF cm<sup>-2</sup>), 10.14 (20.77 mF cm<sup>-2</sup>), and 10.43 F g<sup>-1</sup> (35.46 mF cm<sup>-2</sup>), demonstrating a better charge capability than many reported PVA-based SCs (Xu et al., 2014;

Yun et al., 2014; Su et al., 2015; Chen and Dai, 2016; Li et al., 2017; Wang et al., 2018a; Chen et al., 2019b; Shih et al., 2019; Liu et al., 2020). Furthermore, their GCD curves exhibit a symmetrical triangular shape with a negligible internal resistance (IR) drop, which further proves an ideal reversible capacitance characteristic and small intrinsic resistance from electrodes and electrolyte. Still, the high symmetry of CV curves remains at a wide range of scan rates up to  $100 \text{ mV s}^{-1}$  and GCD plots at various current densities (Figures S12–S14A and S14B) comparable with those employing liquid electrolytes (Adusei et al., 2019; Ahirao et al., 2020), which reveals excellent reaction reversibility and rate capability for all three devices. Based on electrochemical impedance spectra (EIS), Nyquist plots in Figure 2C further reveal the kinetics information of energy storage process. The line nearly parallel to the imaginary axis reflects the ideal capacitive behavior of the devices. The impedance arc associated with the charge transfer resistance ( $R_{ct}$ ) exhibits a value of less than  $1 \Omega$ , indicating a desirable kinetic process even better than many liquid electrolytes-based devices (Guo et al., 2016; Al-Zohbi et al., 2019). At high frequencies, the intercept on the real axis represents the ohmic resistance ( $R_s$ ) of SC-2.5, SC-5.0, and SC-10 being 11.2, 11.5, and 11.7  $\Omega$ , respectively, which assures the good ionic conductivity of PAA-PAH/LiCl electrolyte once again. A slight increase in  $R_s$  with extending PANI deposition time can be ascribed to the deteriorated charge transfer caused by the thickened PANI layer with poor conductivity. Cycle stability is another important feature for the practical application of PAA-PAH electrolyte in SCs. As shown in Figure 2D, after 5,000 charge-discharge cycles at a current density of  $0.2 \text{ mA cm}^{-2}$ , the capacitance retention of SC-2.5, SC-5.0, and SC-10 is 99.95%, 100.0%, and 99.89%, respectively, which presents a superior cycle stability of PAA-PAH/LiCl-based SCs devices than PVA and many other hydrogel electrolytes-based SCs ever reported (Wang et al., 2014a, 2014b, 2018a, 2018b, 2019; Guo et al., 2016; Chen et al., 2019a, 2019b; Liu et al., 2019a, 2019b; Shih et al., 2019; Sun et al., 2019).

Afterward, the regenerability of PAA-PAH/LiCl hydrogel electrolyte was further evaluated by the test of regenerated devices. In a typical device regeneration process, two electrodes were first torn off from the previously used SC-2.5, then gel electrolyte was regenerated in the way described before, and finally these three parts were reassembled into a regenerated device, namely, RSC-2.5. As shown in Figure 3A, the devices before and after regeneration show a slight difference in the shape of their CV plots at a high scan rate of  $50 \text{ mV s}^{-1}$ . On this basis, the specific capacitance of the regenerated device was calculated to be  $6.28 \text{ mF cm}^{-2}$  ( $15.44 \text{ F g}^{-1}$ ), i.e., a slight decrease of 4.85% from the initial state. It suggests the feasibility of this hydrogel electrolyte in the use of device-level regeneration, which can be further confirmed by GCD data, as shown in Figure 3B. The GCD curve of the regenerated device still maintains the ideal symmetrical triangle, similar to the pristine device. Correspondingly, as-calculated specific capacitance of the regenerated device is  $13.90 \text{ mF cm}^{-2}$  ( $17.09 \text{ F g}^{-1}$ ) at  $0.2 \text{ mA cm}^{-2}$ , i.e., 97.61% of the initial state. More CV curves at various scan rates and GCD plots at various current densities of SC-2.5, SC-5.0, SC-10 before and after regeneration can be seen in Figures S12, S14C, and S14D. Based on these GCD curves, as-calculated  $C_a$  values at different discharge current densities are plotted in Figure 3C, where the regenerated device largely retains the specific capacitance of the original device at various discharge currents and shows a small capacitance decay (12.46%) over the discharge rate increase from  $0.2$  to  $2.0 \text{ mA cm}^{-2}$ , close to 10.13% for the pristine device, indicating a well-maintained rate performance. Nyquist plots in Figure 3D may give a clue about the slightly declined capacitance of the regenerated device, where a  $0.25 \Omega$  right shift indicates a minor  $R_s$  increase associated with the deterioration of electrolyte and electrode. Note that the whole device has been regenerated, using electrode that had endured 5,000 repetitive cycles as in the original device and electrolyte subjected to the smash and regeneration. Still, the regenerated device exhibits a capacitance retention of 90.9% after 5,000 repetitive GCD cycles, as illustrated in Figure 3E. So even after one regeneration of the entire device, its cycle stability is still at a leading level among most of PANI-based SCs ever reported (Sivaraman et al., 2010; Yan et al., 2011; He et al., 2012; Liu et al., 2013; Ning et al., 2013; Yu et al., 2014). The last 10 cycles of both devices, shown as Figure 3F, present identical GCD curves with good symmetry and reproducibility, further confirming the superior stability of regenerated device. The small performance attenuation of the regenerated device could result from the intrinsic irreversibility of PANI's pseudocapacity after a long-term use (Liu et al., 2019a), the less-than-100% regeneration efficiency of PAA-PAH/LiCl hydrogel electrolyte as mentioned before, and also the slight mismatch of paper electrode/hydrogel electrolyte interface in the overlapping assembly. Although this is the first report on the regeneration of the whole SC device, the excellent capacitance retention and cycle stability of the regenerated device indicate an ideal electrolyte option applied in highly reliable solid-state electrochemical devices.

To demonstrate the flexibility of the PAA-PAH/LiCl-based SC, the rolling and stretching tests were conducted. After SC-2.5 was rolled into a cylinder, its specific capacitance maintains the original value even with a small enhancement, which can be clearly seen from larger closed area in CV diagrams (Figure 4A)

**Figure 3. Electrochemical Characterization of Regenerated Solid-State Supercapacitor**(A) CV curves of SC-2.5 and RSC-2.5 at a scan rate of  $50 \text{ mV s}^{-1}$ .(B) GCD curves of SC-2.5 and RSC-2.5 at a charge-discharge current density of  $0.2 \text{ mA cm}^{-2}$ .

(C) Areal specific capacitances calculated by GCD curves at different current densities.

(D) Nyquist plots of SC-2.5 and RSC-2.5. Inset: magnified Nyquist plots.

(E) Cycling performance of SC-2.5 and RSC-2.5 for 5,000 cycles.

(F) The last ten GCD cycles of SC-2.5 and RSC-2.5.

and comparable discharge time in GCD plots (Figure 4B). More CV and GCD curves at varied scan rates ( $5\text{--}100 \text{ mV s}^{-1}$ ) and current densities ( $0.2\text{--}2.0 \text{ mA cm}^{-2}$ ) can be found in Figure S16. Accordingly, the  $C_a$  figures of the rolled devices were calculated from their GCD profiles, plotted as in Figure 4C. The  $C_a$  values are almost identical between two states at varied current densities, for instance,  $14.24$  and  $14.43 \text{ mF cm}^{-2}$  at  $0.2 \text{ mA cm}^{-2}$  for the devices before and after rolling, respectively. The small performance enhancement can be attributed to tighter contact between electrodes and hydrogel electrolyte, i.e., smaller interface electrical resistance caused by crimping (Wang et al., 2014a). This can be further evidenced by EIS data in Figure 4D, where the interface resistance for crimped device ( $R_{ct} = 0.3 \Omega$ ) is obviously smaller than the figure at initial state ( $R_{ct} = 0.6 \Omega$ ). On the other hand, a stretchable SC was prepared, where the device stretchability depends on the pre-folded configuration of electrodes (see the device configurations shown in Figure S17A) and the intrinsic excellent stretchability of PAA-PAH gel electrolyte (Chen et al., 2014). To ensure a stable energy storage at the stretching state, the paper electrode was deposited with a small amount of PANI at 1 min. Seen from CV curves and GCD plots (Figures S17B–S17E), the stretched SC reveals an improved capacitance ability as compared with the initial counterpart. At stretching state, for instance, the specific capacitance at a scan rate of  $10 \text{ mV s}^{-1}$  has increased by 58.69% compared with the initial state. It is reasonable to deduce that the unfolded electrodes and simultaneously stretched electrolyte of the stretched device would allow for the expanded interface area and thus the capacitance

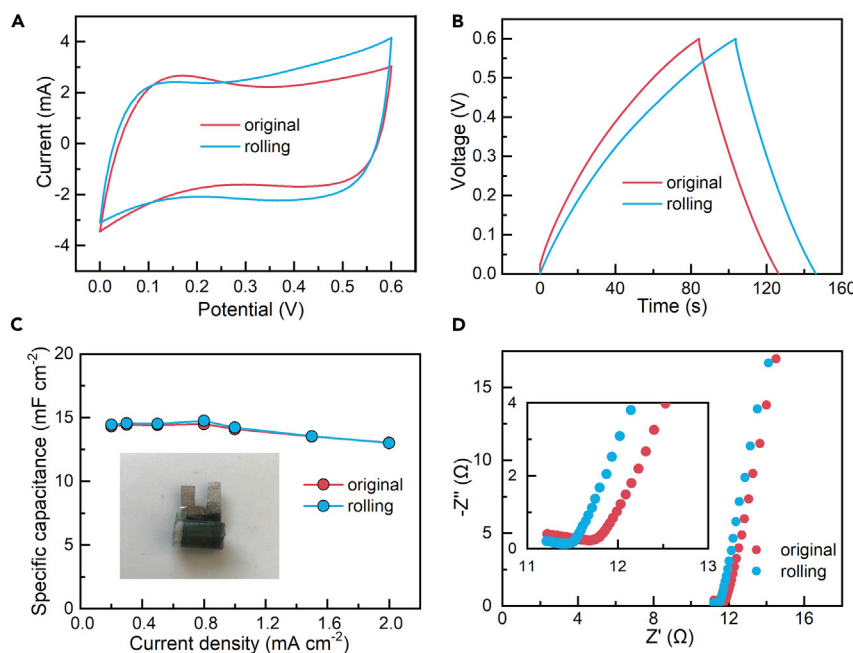


**Figure 4. Electrochemical Characterization of Curled Solid-State Supercapacitor**

- (A) CV curves of SC-2.5 before and after rolling at a scan rate of  $50 \text{ mV s}^{-1}$ .
- (B) GCD curves of SC-2.5 before and after rolling at a charge-discharge current density of  $0.2 \text{ mA cm}^{-2}$ .
- (C) Areal specific capacitances calculated by GCD curves at different current densities. Inset: SC-2.5 at the rolling state.
- (D) Nyquist plots of SC-2.5 before and after rolling. Inset: magnified Nyquist plots.

enhancement as well as the increased interfacial resistance (Figure S17F). Therefore, PAA-PAH hydrogel reveals a highly promising application in flexible SCs that could reliably energize wearable products under natural bending conditions.

In addition, Figure 5A shows the feasible working state of PAA-PAH/LiCl-based SCs that can be assembled in a series or parallel way to widen potential window and enhance energy density, for instance, two SC-2.5 in series can power an electronic timer. Moreover, three series-connected SCs display a voltage window of 1.8 V, triple of a single SC (Figures 5B and 5C), and three parallel-connected SCs exhibit almost triple capacitance (Figures 5B and 5D), indicating a promising practical use of the fabricated solid-state SCs. Based on these outcomes, PAA-PAH/LiCl hydrogel electrolyte is inferred with great potential use in reliable, flexible energy output devices.

## DISCUSSION

In conclusion, we have demonstrated the exploration of an easily regenerable PAA-PAH hydrogel polyelectrolytes with the promising use in reliable, flexible SCs. The PAA-PAH/LiCl electrolyte can be easily pulled to more than 16 times longer and has good ionic conductivity ( $0.050 \text{ S} \cdot \text{cm}^{-1}$ ) and regenerability (96% and 90% of the initial ionic conductivity after the first and second regenerations, respectively). The PAA-PAH/LiCl-based SC retains a high cycling stability (nearly 100% capacitance retention after 5,000 charge-discharge cycles) at static state and even has enhanced capacitances at deformation states such as curling and stretching. The generated SCs made with the regenerated PAA-PAH/LiCl electrolyte and old PANI@CNTs electrodes show indistinctive attenuation in both capacitance retention and cycle stability as compared with the initial state. Moreover, under ambient conditions, it can be easily regenerated or pre-fabricated into highly reliable device components with customized shape and size to fit space and energy needs for a variety of applications, meanwhile avoiding the generation of any environmental problems. Also, the simple manufacturing process with the cheap precursors has laid a solid foundation for industrialization. The present electrolyte may possibly become a standard commercial gel electrolyte and push forward the substantial development of solid-state/flexible electrochemical devices with great reliability and long lifetime.

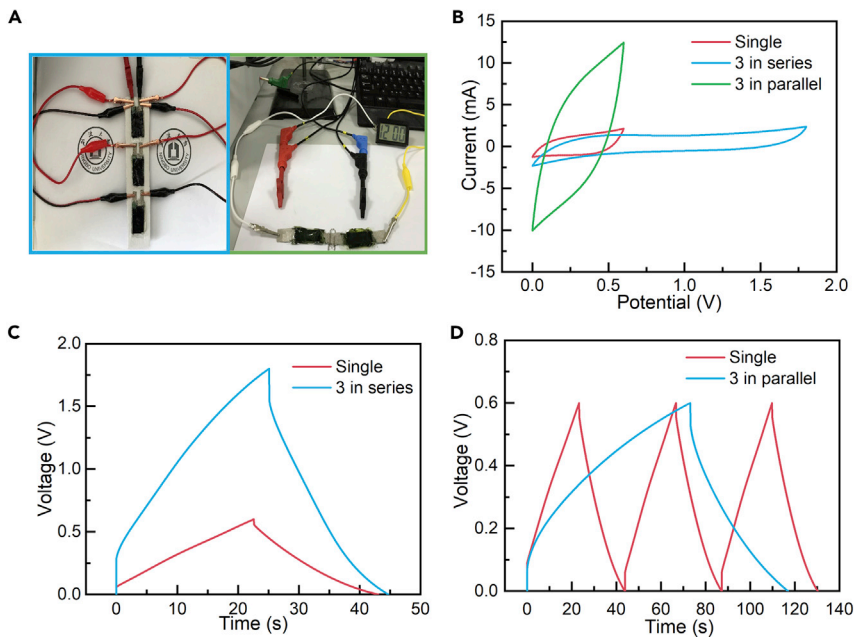


**Figure 5. Electrochemical Characterization of Tandem or Parallel Solid-State Supercapacitors**

(A) The working state of PAA-PAH/LiCl-based SCs.

(B) CV curves of a single device and three devices in series and parallel at a scan rate of  $25 \text{ mV s}^{-1}$ .

(C) GCD curves of a single device and three devices in series at a charge-discharge current density of  $0.5 \text{ mA cm}^{-2}$ .

(D) GCD curves of a single device and three devices in parallel at a charge-discharge current density of  $0.5 \text{ mA cm}^{-2}$ .

### Limitations of the Study

This hydrogel electrolyte exhibits excellent mechanical properties in neutral medium but decreased mechanical properties in strong acid/basic medium owing to the partial fracture of ionic bonds, which would not influence the normal use in quasi-solid-state electrochemical devices but limit the wide application in flexible devices. Therefore, in future work, we would design and prepare the hydrogel electrolyte systems with wider medium adaptability while maintaining the easy processability, regenerability, high ionic conductivity, and ideal operation stability.

### Resource Availability

#### Lead Contact

Further information and requests for resources should be directed to and will be fulfilled by the Lead Contact, Chongyi Chen ([chenchongyi@nbu.edu.cn](mailto:chenchongyi@nbu.edu.cn)).

#### Materials Availability

This study did not generate any new unique reagents.

#### Data and Code Availability

This study did not generate datasets and code.

### METHODS

All methods can be found in the accompanying [Transparent Methods supplemental file](#).

### SUPPLEMENTAL INFORMATION

Supplemental Information can be found online at <https://doi.org/10.1101/101502>.

## ACKNOWLEDGMENTS

This work was supported by National Natural Science Foundation of China (No. 51702176 and 21404062), Zhejiang Provincial Natural Science Foundation of China (No. LY20E020009 and LY20B040003), Natural Science Foundation of Ningbo (No. 2019A610014) and the K. C. Wong Magna Fund in Ningbo University.

## AUTHOR CONTRIBUTIONS

C.C. and Q.L. developed the concept, designed the experiment, and composed the manuscript. G.Z. carried out the experiments, analyzed the data, and wrote the article. All authors provided critical discussion of the data and ideas and gave input on the manuscript.

## DECLARATION OF INTERESTS

The authors declare no competing interests.

Received: June 5, 2020

Revised: August 13, 2020

Accepted: August 20, 2020

Published: September 25, 2020

## REFERENCES

- Adusei, P.K., Kanagaraj, S.N., Gbordzo, S., Jhonson, K., Dearmond, D., Hsieh, Y.Y., Fang, Y., Mishra, S., Phan, N., Alvarez, N., et al. (2019). A scalable nano-engineering method to synthesize 3D-graphene–carbon nanotube hybrid fibers for supercapacitor applications. *Electrochim. Acta* 312, 411–423.
- Ahirao, D.J., Mohanapriya, K., Wilson, H.M., and Jha, N. (2020). Solar reduced porous graphene incorporated within polyaniline network for high-performance supercapacitor electrode. *Appl. Surf. Sci.* 510, 145485.
- Al-Zohbi, F., Jacquemin, J., Ghamouss, F., Schmaltz, B., Abarbri, M., Cherry, K., Tabcheh, M.F., and Tran-Van, F. (2019). Impact of the aqueous pyrrolidinium hydrogen sulfate electrolyte formulation on transport properties and electrochemical performances for polyaniline-based supercapacitor. *J. Power Sources* 431, 162–169.
- Cai, G., Darmawan, P., Cui, M., Wang, J., Chen, J., Magdassi, S., and Lee, P.S. (2016). Highly stable transparent conductive silver grid/PEDOT:PSS electrodes for integrated bifunctional flexible electrochromic supercapacitors. *Adv. Energy Mater.* 6, 1501882.
- Chen, C.R., Qin, H., Cong, H.-P., and Yu, S.-H. (2019a). A highly stretchable and real-time healable supercapacitor. *Adv. Mater.* 31, 1900573.
- Chen, S., Shi, B., He, W., Wu, X., Zhang, X., Zhu, Y., He, S., Peng, H., Jiang, Y., Gao, X., et al. (2019b). Quasifractal networks as current collectors for transparent flexible supercapacitors. *Adv. Funct. Mater.* 29, 1906618.
- Chen, T., and Dai, L. (2016). Flexible and wearable wire-shaped microsupercapacitors based on highly aligned titania and carbon nanotubes. *Energy Storage Mater.* 2, 21–26.
- Chen, T., Xue, Y., Roy, A.K., and Dai, L. (2014). Transparent and stretchable high-performance supercapacitors based on wrinkled graphene electrodes. *ACS Nano* 8, 1039–1046.
- Dai, L., Zhang, W., Sun, L., Wang, X., Jiang, W., Zhu, Z., Zhang, H., Yang, C., and Tang, J. (2019). Highly stretchable and compressible self-healing P(AA-co-AAm)/CoCl<sub>2</sub> hydrogel electrolyte for flexible supercapacitors. *ChemElectroChem* 6, 467–472.
- Eftekhari, A., Li, L., and Yang, Y. (2017). Polyaniline supercapacitors. *J. Power Sources* 347, 86–107.
- Fang, L., Cai, Z., Ding, Z., Chen, T., Zhang, J., Chen, F., Shen, J., Chen, F., Li, R., Zhou, X., et al. (2019). Skin-inspired surface-microstructured tough hydrogel electrolytes for stretchable supercapacitors. *ACS Appl. Mater. Interfaces* 11, 21895–21903.
- Geng, C., Fan, L., Wang, C., Wang, Y., Sun, S., Song, Z., Liu, N., and Wu, J. (2019). High energy density and high working voltage of a quasi-solid-state supercapacitor with a redox-active ionic liquid added gel polymer electrolyte. *New J. Chem.* 43, 18935–18942.
- Guo, Y., Zheng, K., and Wan, P. (2018). A flexible stretchable hydrogel electrolyte for healable all-in-one configured supercapacitors. *Small* 14, 1704497.
- Guo, Y., Zhou, X., Tang, Q., Bao, H., Wang, G., and Saha, P. (2016). A self-healable and easily recyclable supramolecular hydrogel electrolyte for flexible supercapacitors. *J. Mater. Chem. A* 4, 8769–8777.
- He, S., Hu, X., Chen, S., Hu, H., Hanif, M., and Hou, H. (2012). Needle-like polyaniline nanowires on graphite nanofibers: hierarchical micro/nano-architecture for high performance supercapacitors. *J. Mater. Chem.* 22, 5114–5120.
- Hu, C., Zhang, Y., Wang, X., Xing, L., Shi, L., and Ran, R. (2018). Stable, strain-sensitive conductive hydrogel with antifreezing capability, remoldability, and reusability. *ACS Appl. Mater. Interfaces* 10, 44000–44010.
- Hu, J., Xie, K., Liu, X., Guo, S., Shen, C., Liu, X., Li, X., Wang, J.-g., and Wei, B. (2017). Dramatically enhanced ion conductivity of gel polymer electrolyte for supercapacitor via h-BN nanosheets doping. *Electrochim. Acta* 227, 455–461.
- Hu, L., Pasta, M., La Mantia, F., Cui, L., Jeong, S., Deshazer, H.D., Choi, J.W., Han, S.M., and Cui, Y. (2010). Stretchable, porous, and conductive energy textiles. *Nano Lett.* 10, 708–714.
- Huang, Y., Li, H., Wang, Z., Zhu, M., Pei, Z., Xue, Q., Huang, Y., and Zhi, C. (2016). Nanostructured Polypyrrole as a flexible electrode material of supercapacitor. *Nano Energy* 22, 422–438.
- Huang, Y., Zhong, M., Shi, F., Liu, X., Tang, Z., Wang, Y., Huang, Y., Hou, H., Xie, X., and Zhi, C. (2017). An intrinsically stretchable and compressible supercapacitor containing a polyacrylamide hydrogel electrolyte. *Angew. Chem. Int. Ed.* 56, 9141–9145.
- Huang, S., Wan, F., Bi, S., Zhu, J., Niu, Z., and Chen, J. (2019). A self-healing integrated all-in-one zinc-ion battery. *Angew. Chem. Int. Ed.* 58, 4313–4317.
- Kumar, K.S., Choudhary, N., Jung, Y., and Thomas, J. (2018). Recent advances in two-dimensional nanomaterials for supercapacitor electrode applications. *ACS Energy Lett.* 3, 482–495.
- Lee, C.-J., Wu, H., Hu, Y., Young, M., Wang, H., Lynch, D., Xu, F., Cong, H., and Cheng, G. (2018). Ionic conductivity of polyelectrolyte hydrogels. *ACS Appl. Mater. Interfaces* 10, 5845–5852.
- Li, L., Peng, S., Wu, H.B., Yu, L., Madhavi, S., and Lou, X.W. (2015). A flexible quasi-solid-state asymmetric electrochemical capacitor based on hierarchical porous V<sub>2</sub>O<sub>5</sub> nanosheets on carbon nanofibers. *Adv. Energy Mater.* 5, 1500753.
- Li, N., Huang, X., Zhang, H., Li, Y., and Wang, C. (2017). Transparent and self-supporting graphene films with wrinkled-graphene-wall-assembled opening polyhedron building blocks for high performance flexible/transparent supercapacitors. *ACS Appl. Mater. Interfaces* 9, 9763–9771.

Li, H., Han, C., Huang, Y., Huang, Y., Zhu, M., Pei, Z., Xeu, Q., Wang, Z., Liu, Z., Tang, Z., et al. (2018). An extremely safe and wearable solid-state zinc ion battery based on a hierarchical structured polymer electrolyte. *Energy Environ. Sci.* 11, 941–951.

Lin, T., Shi, M., Huang, F., Peng, J., Bai, Q., Li, J., and Zhai, M. (2018). One-pot synthesis of a double-network hydrogel electrolyte with extraordinarily excellent mechanical properties for a highly compressible and bendable flexible supercapacitor. *ACS Appl. Mater. Interfaces* 10, 29684–29693.

Liu, M., Miao, Y.-E., Zhang, C., Tjiu, W.W., Yang, Z., Peng, H., and Liu, T. (2013). Hierarchical composites of polyaniline-graphene nanoribbons-carbon nanotubes as electrode materials in all-solid-state supercapacitors. *Nanoscale* 5, 7312–7320.

Liu, W., Song, M.-S., Kong, B., and Cui, Y. (2017). Flexible and stretchable energy storage: recent advances and future perspectives. *Adv. Mater.* 29, 1603436.

Liu, P., Yan, J., Guang, Z., Huang, Y., Li, X., and Huang, W. (2019a). Recent advancements of polyaniline-based nanocomposites for supercapacitors. *J. Power Sources* 424, 108–130.

Liu, Z., Liang, G., Zhan, Y., Li, H., Wang, Z., Ma, L., Wang, Y., Niu, X., and Zhi, C. (2019b). A soft yet device-level dynamically super-tough supercapacitor enabled by an energy-dissipative dual-crosslinked hydrogel electrolyte. *Nano Energy* 58, 732–742.

Liu, J., Huang, J., Cai, Q., Yang, Y., Luo, W., Zeng, B., Xu, Y., Yuan, C., and Dai, L. (2020). Design of slideable polymer networks: a rational strategy to stretchable, rapid self-healing hydrogel electrolytes for flexible supercapacitors. *ACS Appl. Mater. Inter.* 12, 20479–20489.

Lu, C., and Chen, X. (2020). All-temperature flexible supercapacitors enabled by antifreezing and thermally stable hydrogel electrolyte. *Nano Lett.* 20, 1907–1914.

Lu, N., Na, R., Li, L., Zhang, C., Chen, Z., Zhang, S., Luan, J., and Wang, G. (2020). Rational design of antifreezing organohydrogel electrolytes for flexible supercapacitors. *ACS Appl. Energy Mater.* 3, 1944–1951.

Lu, X., Yu, M., Wang, G., Zhai, T., Xie, S., Ling, Y., Tong, Y., and Li, Y. (2013). H-TiO<sub>2</sub>@MnO<sub>2</sub>//H-TiO<sub>2</sub>@C core-shell nanowires for high performance and flexible asymmetric supercapacitors. *Adv. Mater.* 25, 267–272.

Lu, X., Yu, M., Wang, G., Tong, Y., and Li, Y. (2014). Flexible solid-state supercapacitors: design, fabrication and applications. *Energy Environ. Sci.* 7, 2160–2181.

Luo, F., Sun, T.L., Nakajima, T., Kurokawa, T., Zhao, Y., Sato, K., Ihsan, A.B., Li, X., Guo, H., and Gong, J.P. (2015). Oppositely charged polyelectrolytes form tough, self-healing, and rebuildable hydrogels. *Adv. Mater.* 27, 2722–2727.

Lv, Z., Li, W., Yang, L., Loh, X.J., and Chen, X. (2019). Custom-made electrochemical energy storage devices. *ACS Energy Lett.* 4, 606–614.

Meng, C., Liu, C., Chen, L., Hu, C., and Fan, S. (2010). Highly flexible and all-solid-state paperlike polymer supercapacitors. *Nano Lett.* 10, 4025–4031.

Ning, G., Li, T., Yan, J., Xu, C., Wei, T., and Fan, Z. (2013). Three-dimensional hybrid materials of fish scale-like polyaniline nanosheet arrays on graphene oxide and carbon nanotube for high-performance ultracapacitors. *Carbon* 54, 241–248.

Niu, Z., Zhang, L., Liu, L., Zhu, B., Dong, H., and Chen, X. (2013). All-solid-state flexible ultrathin micro-supercapacitors based on graphene. *Adv. Mater.* 25, 4035–4042.

Oh, J.Y., Rondeau-Gagné, S., Chiu, Y.C., Chortos, A., Lissel, F., Wang, G.N., Schroeder, B.C., Kurosawa, T., Lopez, J., Katsumata, T., et al. (2016). Intrinsically stretchable and healable semiconducting polymer for organic transistors. *Nature* 539, 411–415.

Park, J.M., Jana, M., Nakhanivej, P., Kim, B.-K., and Park, H.S. (2020). Facile multivalent redox chemistries in water-in-bisalt hydrogel electrolytes for hybrid energy storage full cells. *ACS Energy Lett.* 5, 1054–1061.

Peng, H., Lv, Y., Wei, G., Zhou, J., Gao, X., Sun, K., Ma, G., and Lei, Z. (2019). A flexible and self-healing hydrogel electrolyte for smart supercapacitor. *J. Power Sources* 431, 210–219.

Peng, S., Liu, S., Sun, Y., Xiang, N., Jiang, X., and Hou, L. (2018). Facile preparation and characterization of poly(vinyl alcohol)-NaCl-glycerol supramolecular hydrogel electrolyte. *Eur. Polym. J.* 106, 206–213.

Peng, X., Liu, H., Yin, Q., Wu, J., Chen, P., Zhang, G., Liu, G., Wu, C., and Xie, Y. (2016). A zwitterionic gel electrolyte for efficient solid-state supercapacitors. *Nat. Commun.* 7, 11782.

Pomerantseva, E., Bonaccorso, F., Feng, X., Cui, Y., and Gogotsi, Y. (2019). Energy storage: the future enabled by nanomaterials. *Science* 366, 8285.

Qu, G., Li, Y., Yu, Y., Huang, Y., Zhang, W., Zhang, H., Liu, Z., and Kong, T. (2019). Spontaneously regenerative tough hydrogels. *Angew. Chem. Int. Ed.* 58, 10951–10955.

Ray, T.R., Choi, J., Bandodkar, A.J., Krishnan, S., Gutruf, P., Tian, L., Ghaffari, R., and Rogers, J.A. (2019). Bio-integrated wearable systems: a comprehensive review. *Chem. Rev.* 119, 5461–5533.

Ren, Z., Li, Y., and Yu, J. (2018). A flexible supercapacitor with high true performance. *iScience* 9, 138–148.

Shih, C.-C., Lin, Y.-C., Gao, M., Wu, M., Hsieh, H.-C., Wu, N.-L., and Chen, W.-C. (2019). A rapid and green method for the fabrication of conductive hydrogels and their applications in stretchable supercapacitors. *J. Power Sources* 426, 205–215.

Sivaraman, P., Kushwaha, R.K., Shashidhara, K., Hande, V.R., Thakur, A.P., Samui, A.B., and Khandpekar, M.M. (2010). All solid supercapacitor based on polyaniline and crosslinked sulfonated poly(ether ether ketone). *Electrochim. Acta* 55, 2451–2456.

Song, W.-J., Lee, S., Song, G., and Park, S. (2019). Stretchable aqueous batteries: progress and prospects. *ACS Energy Lett.* 4, 177–186.

Su, F., Lv, X., and Miao, M. (2015). High-performance two-ply yarn supercapacitors based on carbon nanotube yarns dotted with Co<sub>3</sub>O<sub>4</sub> and NiO nanoparticles. *Small* 11, 854–861.

Su, H., Zhu, P., Zhang, L., Zeng, W., Zhou, F., Li, G., Li, T., Wang, Q., Sun, R., and Wong, C. (2016). Low cost, high performance flexible asymmetric supercapacitor based on modified filter paper and an ultra-fast packaging technique. *RSC Adv.* 6, 83564–83572.

Sun, K., Feng, E., Zhao, G., Peng, H., Wei, G., Lv, Y., and Ma, G. (2019). A single robust hydrogel film based integrated flexible supercapacitor. *ACS Sustain. Chem. Eng.* 7, 165–173.

Tao, F., Qin, L., Wang, Z., and Pan, Q. (2017). Self-healable and cold-resistant supercapacitor based on a multifunctional hydrogel electrolyte. *ACS Appl. Mater. Inter.* 9, 15541–15548.

Wang, J., Liu, F., Tao, F., and Pan, Q. (2017). Rationally designed self-healing hydrogel electrolyte toward a smart and sustainable supercapacitor. *ACS Appl. Mater. Inter.* 9, 27745–27753.

Wang, K., Zhang, X., Li, C., Sun, X., Meng, Q., Ma, Y., and Wei, Z. (2015). Chemically crosslinked hydrogel film leads to integrated flexible supercapacitors with superior performance. *Adv. Mater.* 27, 7451–7457.

Wang, K., Zhang, X., Li, C., Zhang, H., Sun, X., Xu, N., and Ma, Y. (2014a). Flexible solid-state supercapacitors based on a conducting polymer hydrogel with enhanced electrochemical performance. *J. Mater. Chem. A* 2, 19726–19732.

Wang, X., Liu, B., Liu, R., Wang, Q., Hou, X., Chen, D., Wang, R., and Shen, G. (2014b). Fiber-based flexible all-solid-state asymmetric supercapacitors for integrated photodetecting system. *Angew. Chem. Int. Ed.* 53, 1849–1853.

Wang, Z., Tao, F., and Pan, Q. (2016). A self-healable polyvinyl alcohol-based hydrogel electrolyte for smart electrochemical capacitors. *J. Mater. Chem. A* 4, 17732–17739.

Wang, Y., Pei, Z., Zhu, M., Liu, Z., Huang, Y., Ruan, Z., Huang, Y., Zhao, Y., Du, S., and Zhi, C. (2018a). A wearable supercapacitor engaged with gold leaf gilding cloth toward enhanced practicability. *ACS Appl. Mater. Interfaces* 10, 21297–21305.

Wang, Z., Li, H., Tang, Z., Liu, Z., Ruan, Z., Ma, L., Yang, Q., Wang, D., and Zhi, C. (2018b). Hydrogel electrolytes for flexible aqueous energy storage devices. *Adv. Funct. Mater.* 28, 1804560.

Wang, S., Xu, J., Wang, W., Wang, G.N., Rastak, R., Molina-Lopez, F., Chung, J.W., Niu, S., Feig, V.R., Lopez, J., Lei, T., et al. (2018c). Skin electronics from scalable fabrication of an intrinsically stretchable transistor array. *Nature* 555, 83–88.

Wang, Y., Chen, F., Liu, Z., Tang, Z., Yang, Q., Zhao, Y., Du, S., Chen, Q., and Zhi, C. (2019). A highly elastic and reversibly stretchable all-polymer supercapacitor. *Angew. Chem. Int. Ed.* 58, 15707–15711.

- Wang, Z., Zhu, M., Pei, Z., Xue, Q., Li, H., Huang, Y., and Zhi, C. (2020). Polymers for supercapacitors: boosting the development of the flexible and wearable energy storage. *Mater. Sci. Eng. R* 139, 100520.
- Xu, P., Gu, T., Cao, Z., Wei, B., Yu, J., Li, F., Byun, J.-H., Lu, W., Li, Q., and Chou, T.-W. (2014). Carbon nanotube fiber based stretchable wire-shaped supercapacitors. *Adv. Energy Mater.* 4, 1300759.
- Xue, Q., Sun, J., Huang, Y., Zhu, M., Pei, Z., Li, H., Wang, Y., Li, N., Zhang, H., and Zhi, C. (2017). Recent progress on flexible and wearable supercapacitors. *Small* 13, 1701827.
- Yan, Y., Cheng, Q., Wang, G., and Li, C. (2011). Growth of polyaniline nanowiskers on mesoporous carbon for supercapacitor application. *J. Power Sources* 196, 7835–7840.
- Yang, J., Yu, X., Sun, X., Kang, Q., Zhu, L., Qin, G., Zhou, A., Sun, G., and Chen, Q. (2020). Polyaniline-decorated supramolecular hydrogel with tough, fatigue-resistant, and self-healable performances for all-in-one flexible supercapacitors. *ACS Appl. Mater. Interfaces* 12, 9736–9745.
- Ye, T., Li, D., Liu, H., She, X., Xia, Y., Zhang, S., Zhang, H., and Yang, D. (2018). Seaweed biomass-derived flame-retardant gel electrolyte membrane for safe solid-state supercapacitors. *Macromolecules* 51, 9360–9367.
- Yu, P., Zhao, X., Huang, Z., Li, Y., and Zhang, Q. (2014). Free-standing three-dimensional graphene and polyaniline nanowire arrays hybrid foams for high-performance flexible and lightweight supercapacitors. *J. Mater. Chem. A* 2, 14413–14420.
- Yuan, T., Cui, X., Liu, X., Qu, X., and Sun, J. (2019a). Highly tough, stretchable, self-healing, and recyclable hydrogels reinforced by in situ-formed polyelectrolyte complex nanoparticles. *Macromolecules* 52, 3141–3149.
- Yuan, T., Qu, X., Cui, X., and Sun, J. (2019b). Self-healing and recyclable hydrogels reinforced with in situ-formed organic nanofibrils exhibit simultaneously enhanced mechanical strength and stretchability. *ACS Appl. Mater. Interfaces* 11, 32346–32353.
- Yun, J., Kim, D., Lee, G., and Ha, J.S. (2014). All-solid-state flexible micro-supercapacitor arrays with patterned graphene/MWNT electrodes. *Carbon* 79, 156–164.
- Zhang, X., Wang, L., Peng, J., Cao, P., Cai, X., Li, J., and Zhai, M. (2015). A flexible ionic liquid gelled PVA-Li<sub>2</sub>SO<sub>4</sub> polymer electrolyte for semi-solid-state supercapacitors. *Adv. Mater. Interfaces* 2, 1500267.
- Zhao, J., Chen, Y., Yao, Y., Tong, Z., Li, P., Yang, Z., and Jin, S. (2018). Preparation of the polyelectrolyte complex hydrogel of biopolymers via a semi-dissolution acidification sol-gel transition method and its application in solid-state supercapacitors. *J. Power Sources* 378, 603–609.
- Zhou, Y., Wan, C., Yang, Y., Yang, H., Wang, S., Dai, Z., Ji, K., Jiang, H., Chen, X., and Long, Y. (2019). Highly stretchable, elastic, and ionic conductive hydrogel for artificial soft electronics. *Adv. Funct. Mater.* 29, 1806220.

## **Supplemental Information**

### **A Regenerable Hydrogel Electrolyte for Flexible Supercapacitors**

**Guanbing Zhou, Leyi Yang, Weijun Li, Chongyi Chen, and Qiao Liu**

## **Transparent Methods**

**Materials:** Acrylic acid (AA), ammonium persulfate (APS), lithium chloride (LiCl) and polyvinyl alcohol (PVA) 1799 were purchased from Aladdin Reagent Co., Ltd. Shanghai, China. Lithium hydroxide (LiOH) was purchased from Innochem Science and Technology Co., Ltd. Beijing, China. Aniline was obtained from Macklin Reagent Co., Ltd. Shanghai, China. Polyallylamine hydrochloride (PAH) was purchased from Suzhou Tianke Trading Co., Ltd. Carbon nanotube film was purchased from Timesnano Co., Ltd. Chengdu, China. Acrylic acid was purified by vacuum distillation before use. Unless otherwise noted, all reagents were used as received.

**Preparation of PAA-PAH/LiCl hydrogel electrolyte:** AA lithium salt (0.060 mol) and PAH (0.060 mol) were dissolved slowly by stirring in water (30 mL) at 0 °C, followed by the addition of LiCl (0.030 mol). Then, APS (1.5 wt% of AA) was added to the above aqueous solution and bubbling with nitrogen to remove oxygen. Thereafter, the above solution was transferred into a mold ( $10 \times 10 \times 0.3 \text{ cm}^3$ ) and evacuated to remove the dissolved air in solution. Finally, the solution was held at room temperature for 12 h to form PAA-PAH/LiCl gel electrolyte.

**Regeneration of PAA-PAH/LiCl hydrogel electrolyte:** Firstly, PAA-PAH/LiCl hydrogel electrolyte was lyophilized and the as-obtained cryogel was grinded into hundred-micrometer fine powder. Next, the cryogel powder was placed in a specific mold, following by the addition of water. After regenerating for 12 h at room temperature, the regenerated PAA-PAH/LiCl hydrogel electrolyte was obtained.

**Preparation of PVA/LiCl hydrogel electrolyte:** PVA (0.060 mol) was dissolved slowly by stirring in water (25 mL) at 85 °C, followed by the addition of LiCl (0.075 mol). The above solution was transferred into a mold ( $10 \times 10 \times 0.3 \text{ cm}^3$ ) and sealed. It was stored at -20 °C for 12 h, and then thawed at room temperature for another 12 h. After three freeze-thaw cycles, PVA/LiCl hydrogel electrolyte was obtained.

**Preparation of PANI@CNT electrodes and assembly of supercapacitors:** Flexible electrodes were prepared by electrochemically depositing PANI on CNT papers at 0.8 V (vs. Ag/AgCl) for 1.0, 2.5, 5.0, 7.5, 10, 15 min in an aqueous solution of 1M HCl and 1wt% aniline monomer at room temperature. Two identical PANI@CNT electrodes were coated onto the opposite sides of PAA-PAH/LiCl hydrogel electrolyte to assemble a supercapacitor prototype ( $1.0 \times 3.0 \times 0.3 \text{ cm}^3$ ).

**Methods:** The structure of lyophilized PAA-PAH/LiCl gel electrolyte and PANI@CNT paper electrodes was observed by using a field-emission scanning electron microscope (FE-SEM, S-4800, Hitachi, Japan). The regeneration process was recorded on a 3D microscope (KEYENCE, VH-5500k, Japan). The mechanical properties of the PAA-PAH/LiCl gel electrolytes (diameter = 4.0 mm) were measured on a tensile testing machine (Shenzhen Kaiqiangli Testing Instruments KD III-0.05, China) at room temperature (stretching speed =  $50 \text{ mm min}^{-1}$ ). The engineering tensile stress ( $\sigma$ ) was calculated by  $\sigma = L/(\pi R^2)$ , where  $L$  is the load and  $R$  is the initial radius of the sample.

The engineering tensile strain ( $\varepsilon$ ) was defined as the change in length ( $l$ ) relative to the initial gauge length ( $l_0$ ) of the sample,  $\varepsilon = l/l_0 \times 100\%$ . The toughness was calculated by the area under the stress-strain curve. Fourier transform infrared (FTIR) spectrum of all samples was taken using a Nicolet 460 IR spectrometer, and the sample was examined in pressed KBr pellets (the cryogel powder was mixed with KBr in 1%wt).

The electrochemical behavior of the assembled supercapacitors was evaluated by cyclic voltammetry (CV), electrochemical impedance spectroscopy (EIS), and galvanostatic charge/discharge (GCD) measurements on an electrochemical station (Autolab PGSTAT302N, Switzerland). Electrochemical impedance spectroscopy was performed in the frequency range of  $10^2$ – $10^5$  Hz with a magnitude of 5 mV at open circuit voltage. Cycle stability tests were conducted by a Land 2001A battery testing system. The specific capacitance ( $C_s$ ) of the supercapacitor was calculated by  $C_a = (I \times t)/(\Delta V \times S)$ ,  $C_s = (I \times t)/(\Delta V \times m)$ , where  $I$ ,  $t$ ,  $\Delta V$ ,  $S$  and  $m$  are discharge current density, discharge time, voltage window, the electrode area or PANI mass, respectively. The ionic conductivity of PAA-PAH/LiCl gel electrolyte was determined from electrochemical impedance spectra (EIS), where a piece of hydrogel electrolyte was sandwiched by two pieces of platinum sheets of  $15 \times 15$  mm $^2$  and the ionic conductivity value  $s$  (S cm $^{-1}$ ) was calculated by the equation  $s = L/(R_b \times A)$ , where  $L$  is the thickness (cm) of the hydrogel,  $A$  is the contact area (cm $^2$ ) of the hydrogel with the current collectors, and  $R_b$  is the bulk resistance obtained from the first intercept on the x-axis of the impedance plots.

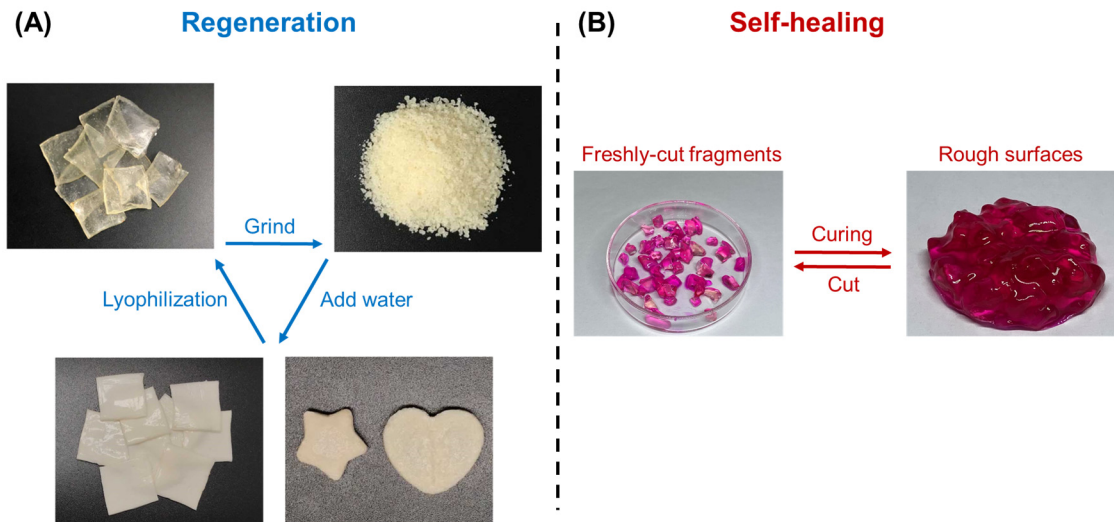


**Figure S1.** Digital images illustrating the experimental processes for (A) the regeneration of hydrogel electrolyte and (B) the self-healing of same hydrogel dyed with Rhodamine B, respectively. Accordingly, the difference between the regeneration and the self-healing can be understood. The self-heal process involves the direct contact between incisions of two or several separate hydrogel pieces (Self-Healing Hydrogels. Adv. Mater. 2016, 28, 9060-9093), while the regeneration of hydrogel (Spontaneously Regenerative Tough Hydrogels. Angew. Chem. Int. Ed. 2019, 58, 10951-10955) comprises the lyophilizing of hydrogel, grinding of cryogel, swelling of cryogel particles in water, and finally fusing of hydrogel particles, which involves the restoring of numerous interfaces. Related to Figure 1.

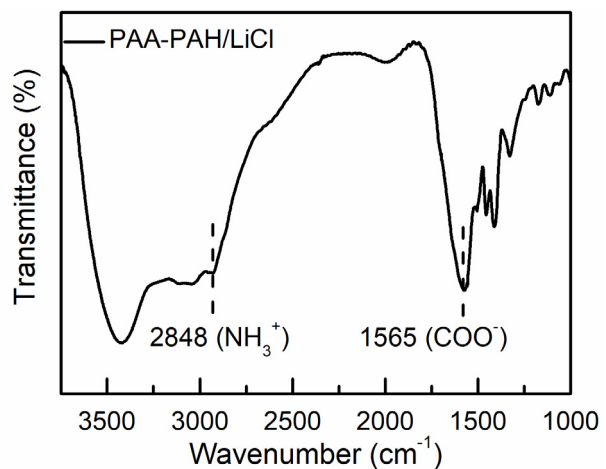


**Figure S2.** FTIR spectrum of lyophilized PAA-PAH/LiCl gel electrolyte. Related to Figure 1.

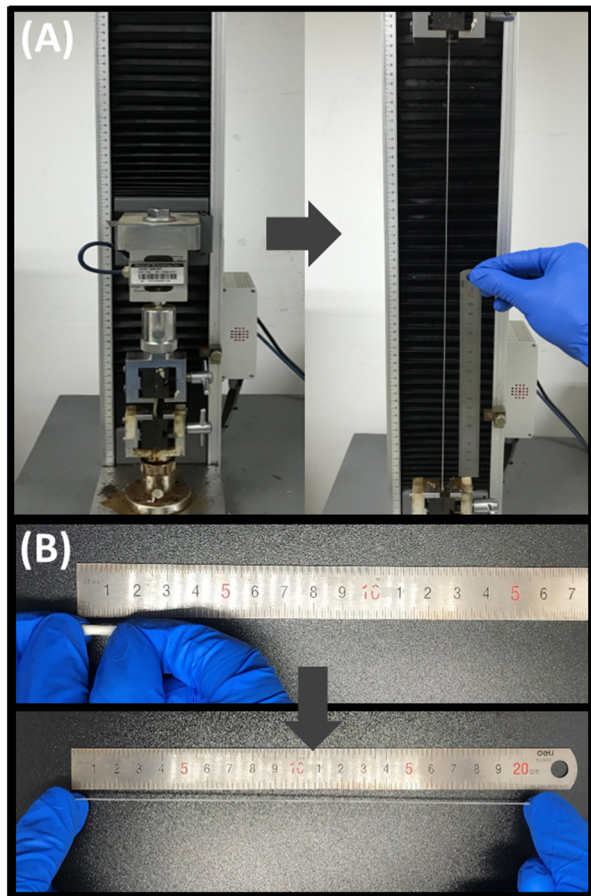


**Figure S3.** Digital photographs demonstrate the extensibility of PAA-PAH/LiCl hydrogel. Related to Figure 1.

**Table S1.** Overview of ionic conductivity of reported hydrogel electrolytes for energy storage devices. Related to Figure 1.

Gel system <sup>a</sup> (Cross-links)	Electrolyte salt added	Ionic conductivity/ S cm <sup>-1</sup>	Ref
PAAm (Covalent bond)	1M KCl	0.050	(Tang, Chen et al. 2015)
PAAm (Covalent bond)	1M Li <sub>2</sub> SO <sub>4</sub>	0.0535	(Wei, Zhou et al. 2018)
Gelatin-g-PAAm (Covalent bond)	2M ZnSO <sub>4</sub>	0.0176	(Li, Han et al. 2018)
PVA-g-PAA (Dynamic covalent bond)	1M KCl	0.041	(Wang, Tao et al. 2016)
PVA/GO (Dynamic covalent bond)	2M KCl	0.0475	(Peng, Lv et al. 2019)
PAA-co-PAAm (Ionic bond)	1M KCl	0.017	(Dai, Zhang et al. 2019)
CTS-SA (Ionic bond)	2.2 mol kg <sup>-1</sup> NaCl	0.051	(Zhao, Chen et al. 2018)
PAAm (Hydrogen bond)	0.5M Na <sub>2</sub> SO <sub>4</sub>	0.036	(Tang, Chen et al. 2015)
Li-Alg (Hydrogen bond)	2M LiOAc	0.0326	(Ye, Li et al. 2018)
PVA (Hydrogen bond)	2M Zn(CF <sub>3</sub> SO <sub>3</sub> ) <sub>2</sub>	0.0126	(Huang, Wan et al. 2019)
HPC/PVA (Hydrogen bond)	5M NaCl	0.034	(Zhou, Wan et al. 2019)
AG/PAAm (Covalent bond/ Hydrogen bond)	1 mol kg <sup>-1</sup> LiCl	0.013	(Fang, Cai et al. 2019)
Alg/PAAm (Covalent bond/ Ionic bond)	1M Li <sub>2</sub> SO <sub>4</sub>	0.029	(Liu, Liang et al. 2019)
Li-AG/PAAm (Covalent bond/ Hydrogen bond)	1.2 mol kg <sup>-1</sup> Li <sub>2</sub> SO <sub>4</sub>	0.041	(Lin, Shi et al. 2018)
PolyVI-HPA (Covalent bond/ Hydrogen bond)	3M NaNO <sub>3</sub>	0.016 (-15°C), 0.0596 (45°C)	(Wang, Liu et al. 2017)
PVA (Hydrogen bond/ Dynamic covalent bond)	3M KCl	0.038	(Sun, Feng et al. 2019)
HPC/PVA (Hydrogen bond)	2M LiClO <sub>4</sub>	0.0273	(Lu, Na et al. 2020)
PEI-PVA-Bn (Hydrogen bond/ Dynamic covalent bond)	0.4 mol kg <sup>-1</sup> LiCl	0.02149	(Liu, Huang et al. 2020)
MMT/PVA (Hydrogen bond)	2M H <sub>2</sub> SO <sub>4</sub>	0.17×10 <sup>-4</sup> (-50°C), 0.76×10 <sup>-4</sup> (90°C)	(Lu and Chen 2020)
PVA-Pyr <sub>14</sub> Br (Hydrogen bond)	0.28M Na <sub>2</sub> SO <sub>4</sub>	0.0271	(Geng, Fan et al. 2019)
<b>PAA-PAH (Ionic bond)</b>	<b>1M LiCl</b>	<b>0.050</b>	<b>This work</b>

<sup>a</sup> **PAAm:** Polyacrylamide; **PAA:** Polyacrylic acid; **PVA:** Polyvinyl alcohol; **CTS:** Chitosan, **SA:** Sodium alginate; **Alg:** Alginate; **HPC:** Hydroxypropyl cellulose; **AG:** Agar; **VI:** Vinylimidazole; **HPA:** Hydroxypropyl acrylate; **PEI:** Polyethyleneimine; **Bn:** 4-formylphenylboronic acid; **MMT:** Montmorillonite; **Pyr<sub>14</sub>Br:** N-butyl-N-methylpyrrolidinium bromide.

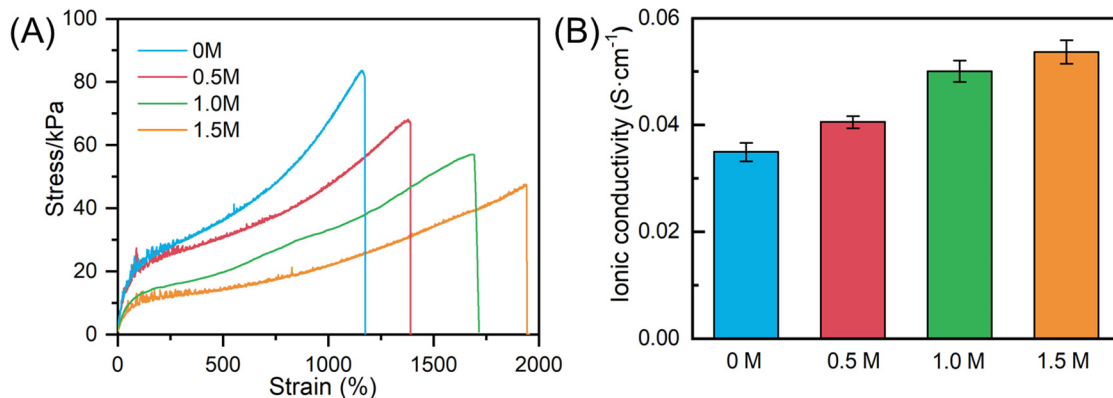


**Figure S4.** (A) The mechanical property and (B) ionic conductivity of PAA-PAH/LiCl with different concentration of LiCl addition. 1.0 M extra addition was chosen as a trade-off between mechanical property and ionic conductivity. Related to Figure 1.

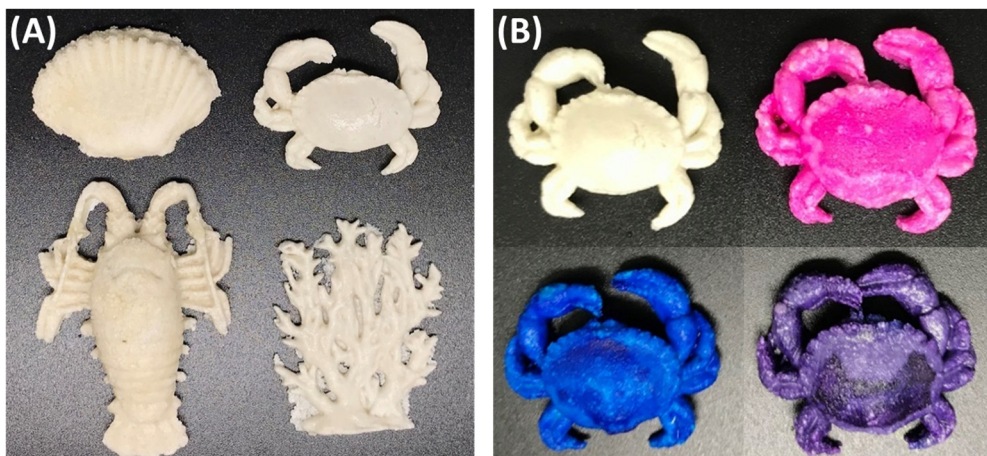


**Figure S5.** Regenerated PAA-PAH/LiCl hydrogel electrolyte (A) with various shapes and (B) in different colors. Related to Figure 1.

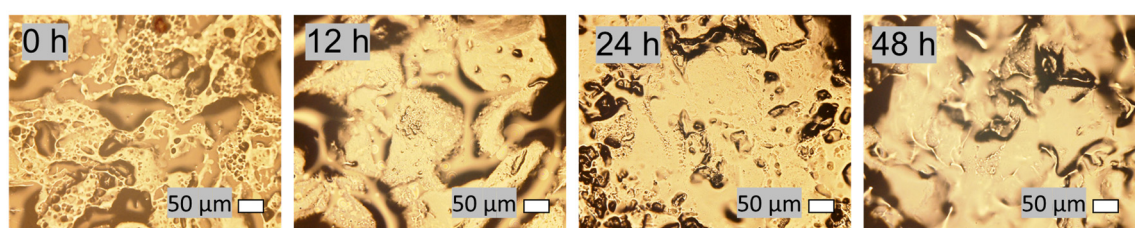


**Figure S6.** The 3D microscope images showing the regeneration process of PAA-PAH/LiCl

hydrogel electrolyte. Related to Figure 1.

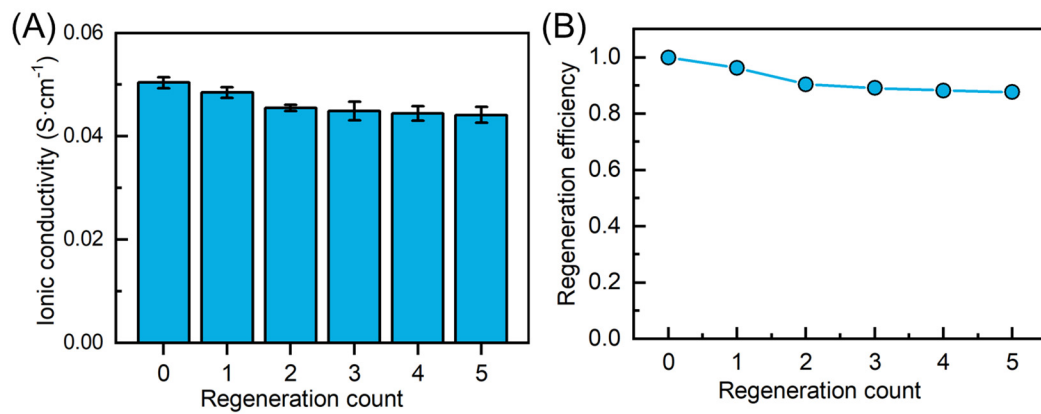


**Figure S7.** (A) The ionic conductivity, (B) regeneration efficiency of ionic conductivity of PAA-PAH/LiCl after different regeneration count. Related to Figure 1.

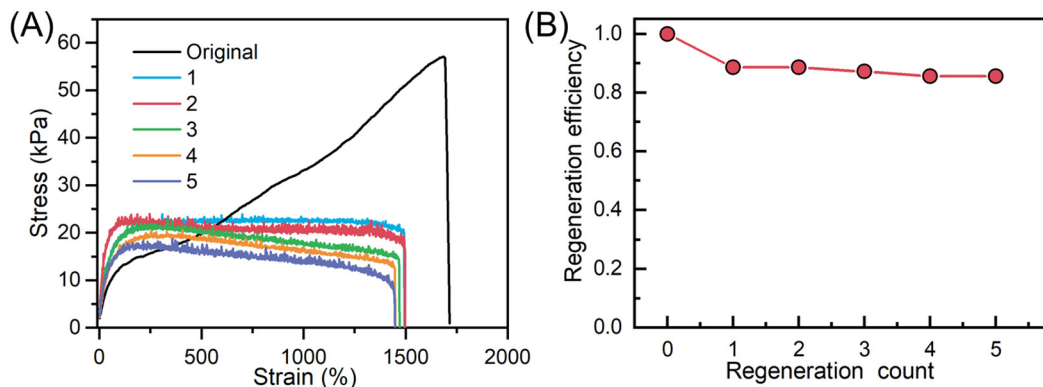


**Figure S8.** (A) Stress-strain curves, (B) regeneration efficiency based on fractural strain of PAA-PAH/LiCl after different regeneration count. Related to Figure 1.

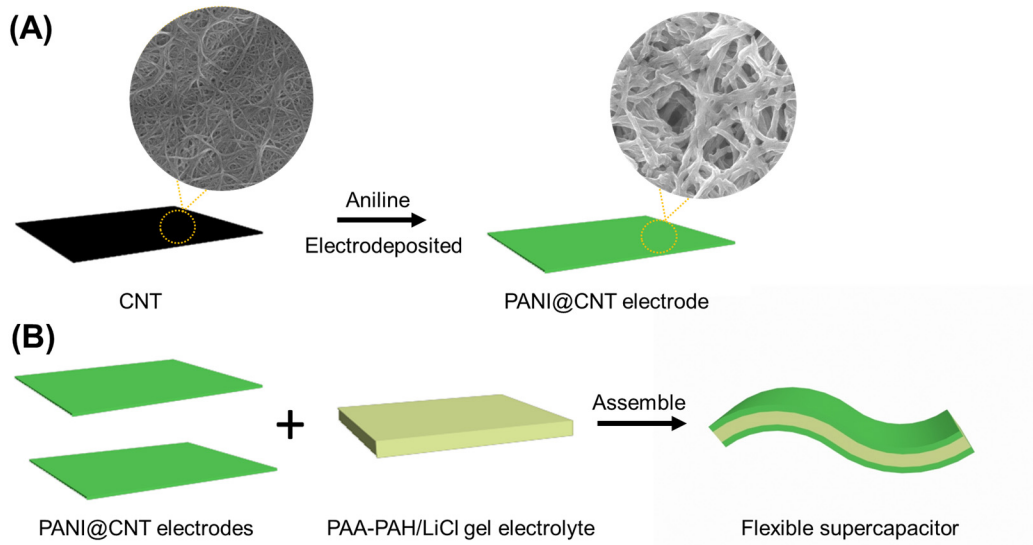


**Figure S9.** Schematic diagram of (A) the preparation of PANI@CNTs electrode and (B) the assembly of the flexible supercapacitor. Related to Figure 2.

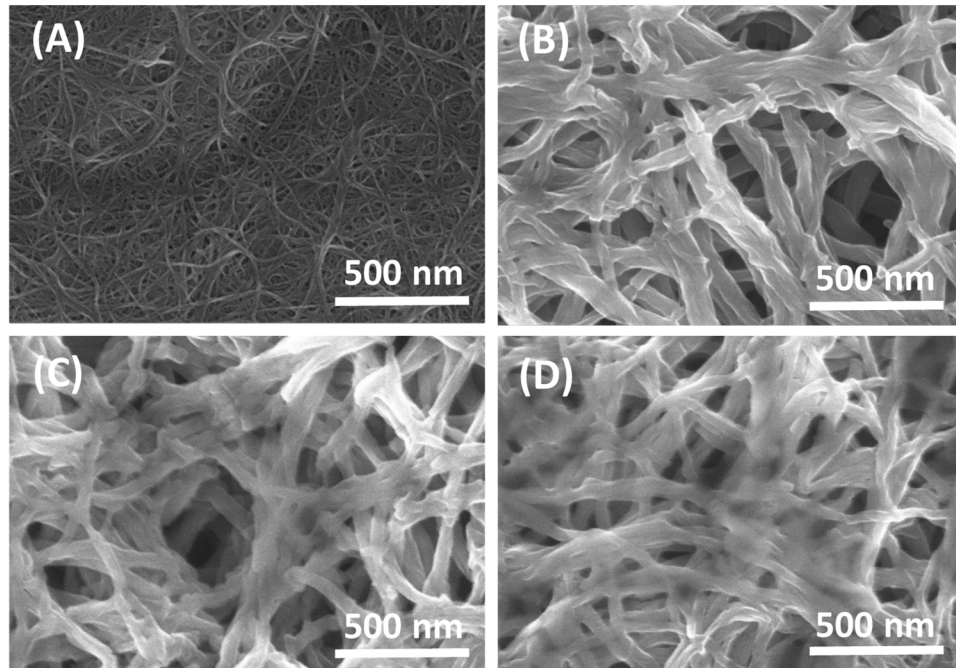


**Figure S10.** SEM images of the PANI@CNTs electrodes with the PANI deposition time of (A) 0 min, (B) 5.0 min, (C) 10 min and (D) 15 min. Related to Figure 2.

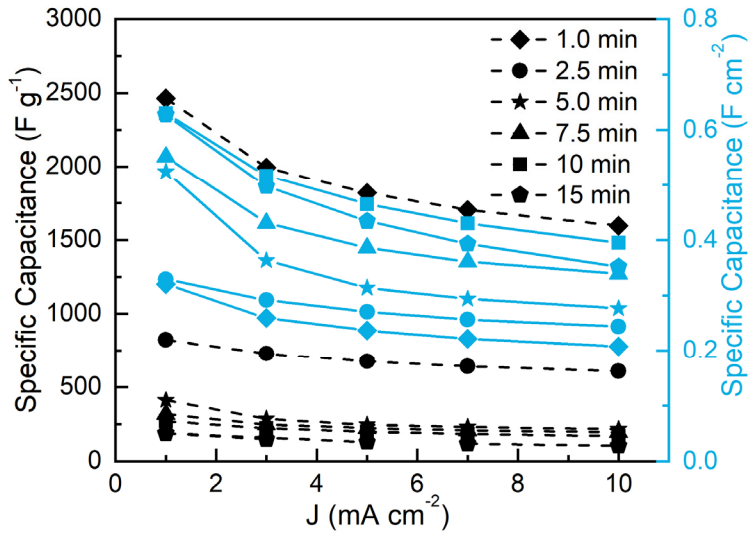


**Figure S11.** Specific capacitance of PANI@CNTs electrodes at different deposition time. Related to Figure 2.

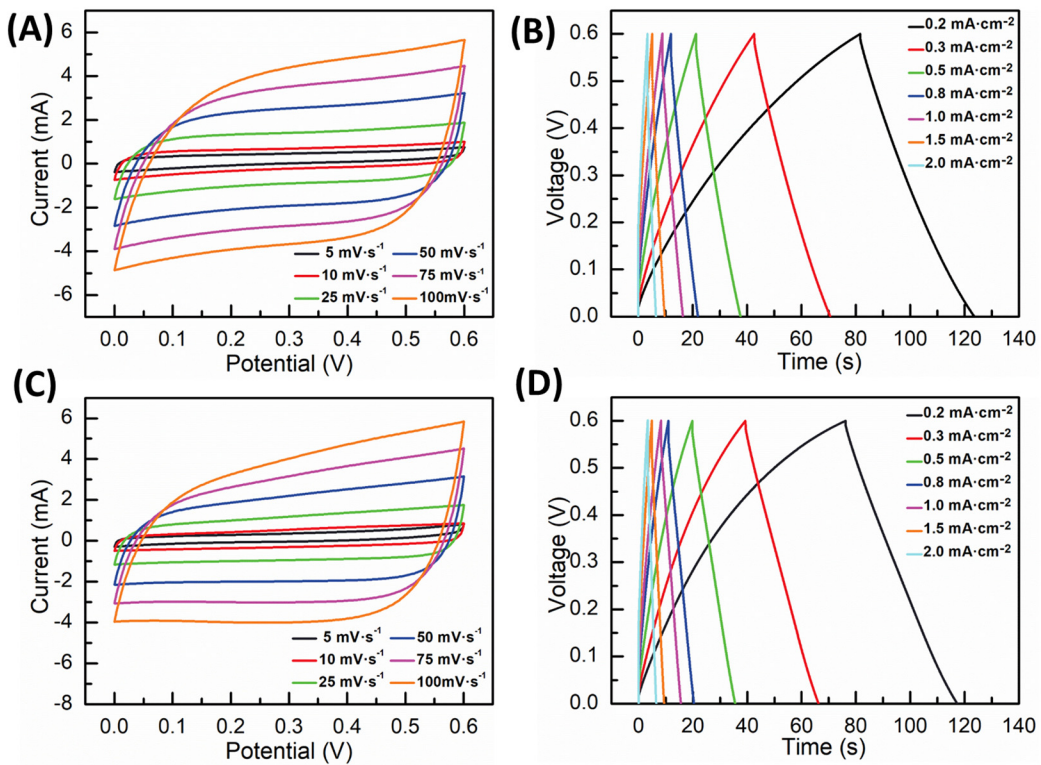


**Figure S12.** (A) CV and (B) GCD curves of SC-2.5, (C) CV and (D) GCD curves of RSC-2.5. Related to Figure 3.

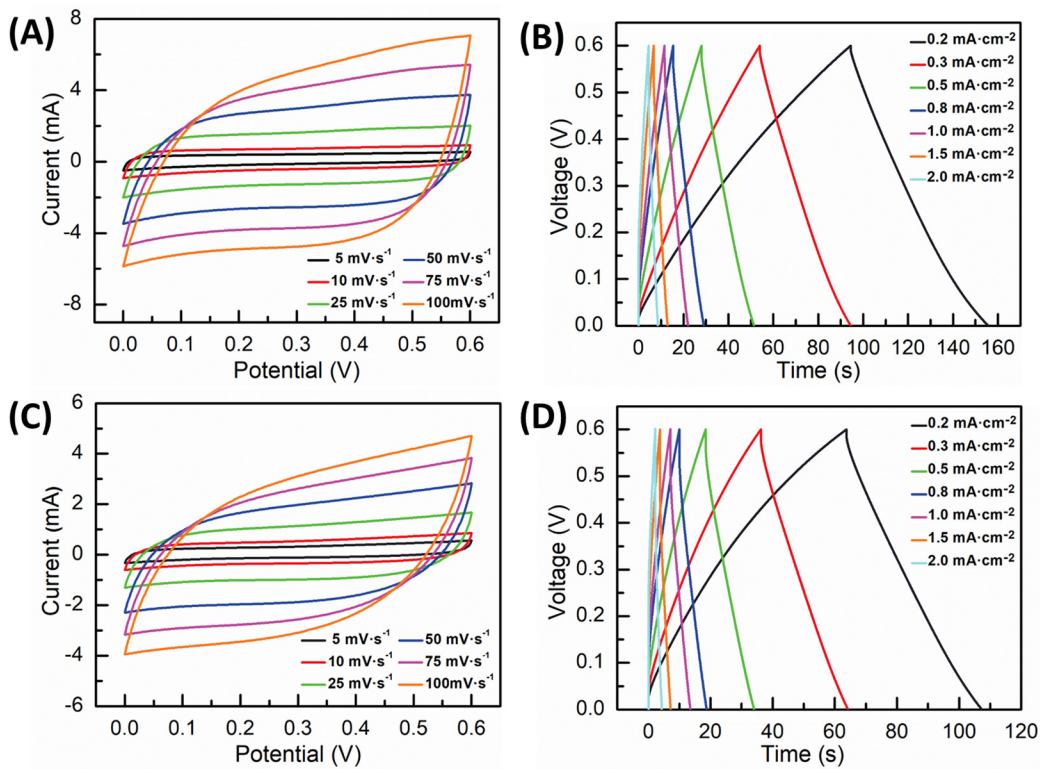


**Figure S13.** (A) CV and (B) GCD curves of SC-5.0, (C) CV and (D) GCD curves of RSC-5.0.  
Related to Figure 3.

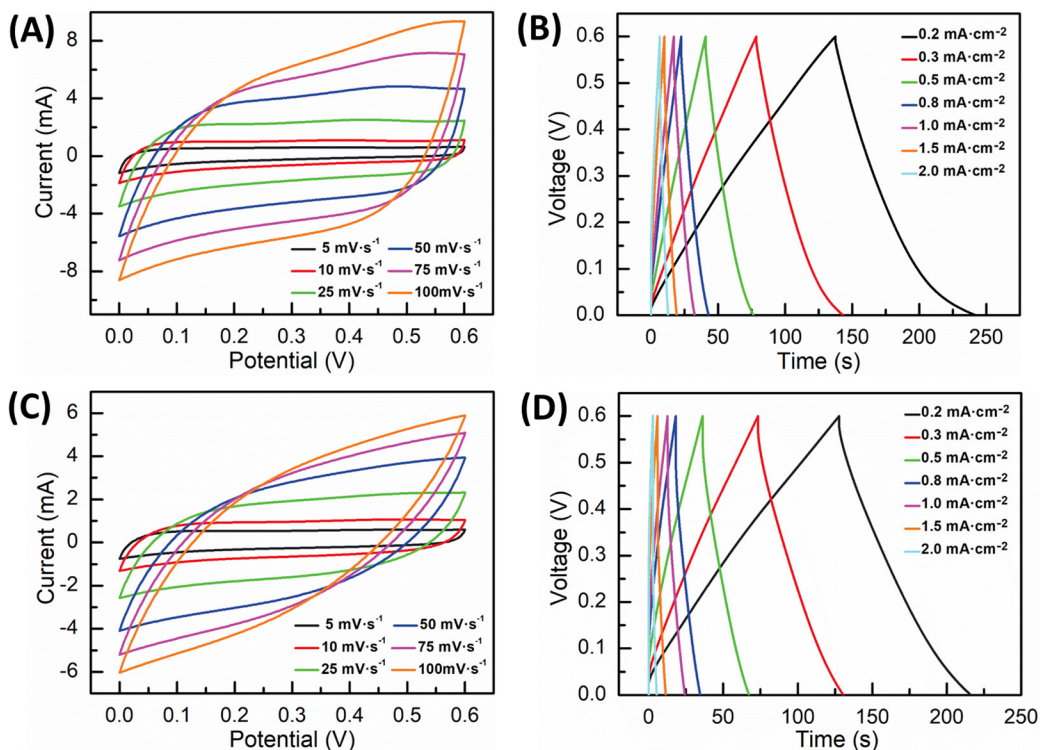


**Figure S14.** (A) CV and (B) GCD curves of SC-10, (C) CV and (D) GCD curves of RSC-10.

Related to Figure 3.

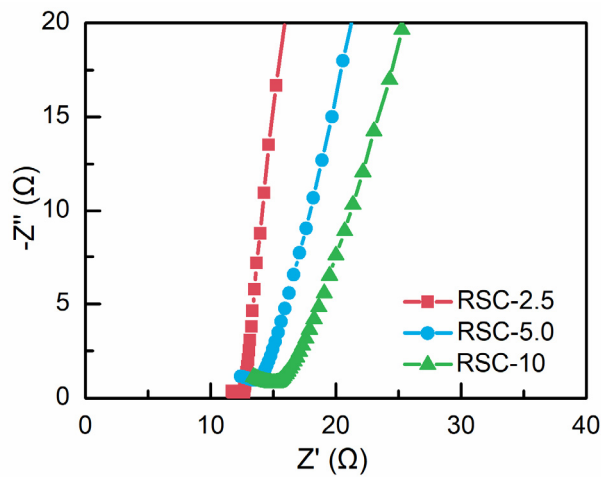


**Figure S15.** Nyquist plots of RSC-2.5, RSC-5.0 and RSC-10. Related to Figure 3.

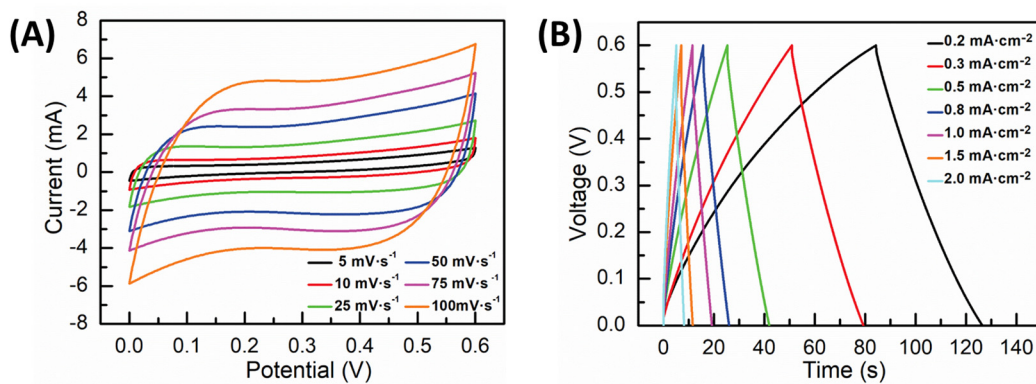


**Figure S16.** (A) CV curves at different scan rates and (B) GCD curves under different charge-discharge current densities of supercapacitor at the rolling state. Related to Figure 4.

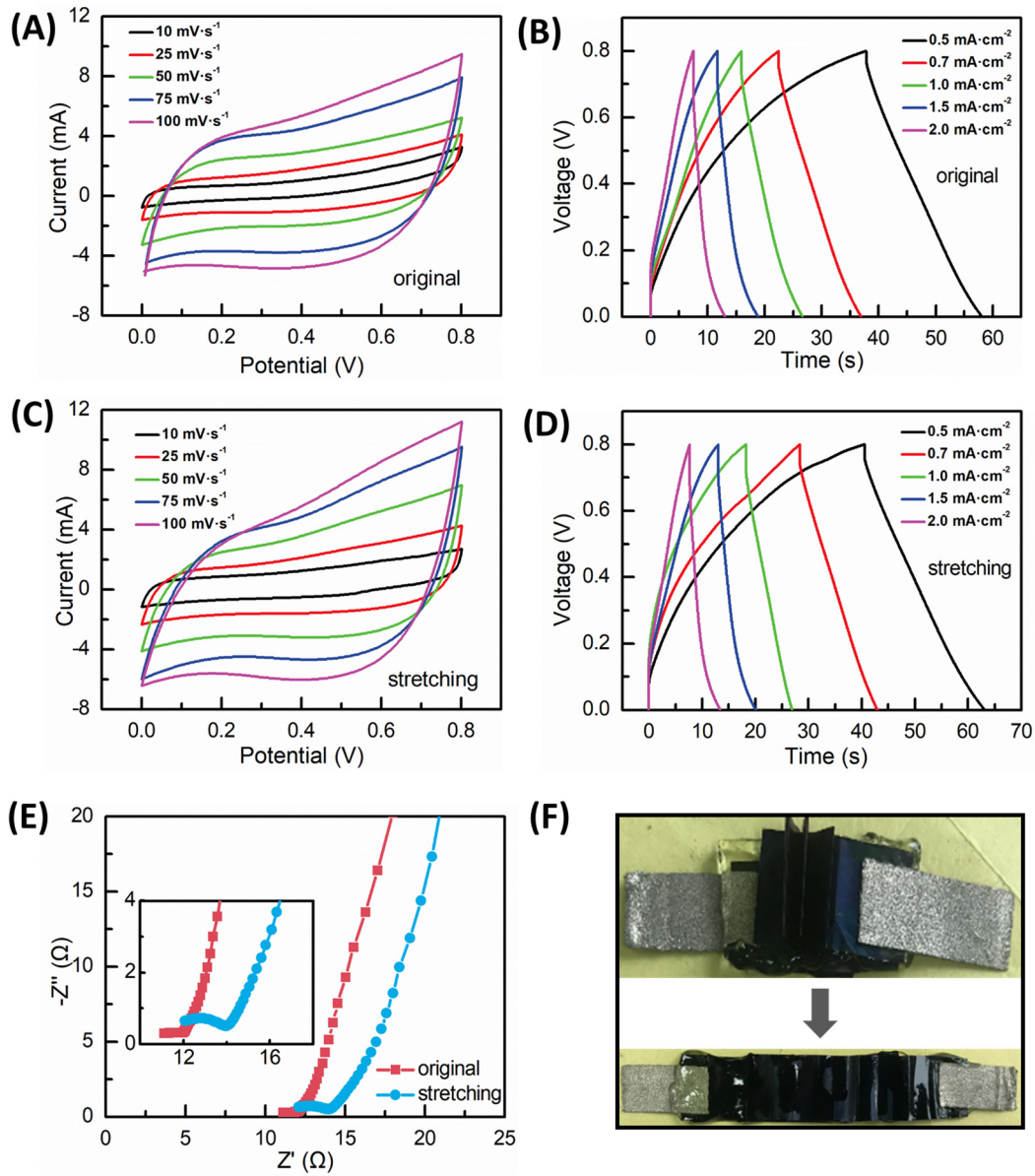


**Figure S17.** Electrochemical performance of supercapacitors before and after stretching: (A) CV curves at different scan rates and (B) GCD curves under different charge-discharge current densities of supercapacitor before stretching, (C) CV curves at different scan rates and (D) GCD curves under different charge-discharge current densities of supercapacitor after stretching, (E) their Nyquist plots and (F) digital photos showing the device configurations at original and stretching states. Related to Figure 4.

## REFERENCES

Dai, L., Zhang, W., Sun, L., Wang, X., Jiang, W., Zhu, Z., Zhang, H., Yang, C. and Tang, J. (2019). Highly Stretchable and Compressible Self-Healing P(AA-co-AAm)/CoCl<sub>2</sub> Hydrogel Electrolyte for Flexible Supercapacitors.

- ChemElectroChem 6, 467-472.
- Fang, L., et al. (2019). Skin-Inspired Surface-Microstructured Tough Hydrogel Electrolytes for Stretchable Supercapacitors. *ACS Appl. Mater. Interfaces* 11, 21895-21903.
- Geng, C., Fan, L., Wang, C., Wang, Y., Sun, S., Song, Z., Liu, N. and Wu, J. (2019). High energy density and high working voltage of a quasi-solid-state supercapacitor with a redox-active ionic liquid added gel polymer electrolyte. *New J. Chem.* 43, 18935-18942.
- Huang, S., Wan, F., Bi, S., Zhu, J., Niu, Z. and Chen, J. (2019). A Self-Healing Integrated All-in-One Zinc-Ion Battery. *Angew. Chem. Int. Ed.* 58, 4313-4317.
- Li, H., et al. (2018). An extremely safe and wearable solid-state zinc ion battery based on a hierarchical structured polymer electrolyte. *Energy Environ. Sci.* 11, 941-951.
- Lin, T., Shi, M., Huang, F., Peng, J., Bai, Q., Li, J. and Zhai, M. (2018). One-Pot Synthesis of a Double-Network Hydrogel Electrolyte with Extraordinarily Excellent Mechanical Properties for a Highly Compressible and Bendable Flexible Supercapacitor. *ACS Appl. Mater. Interfaces* 10, 29684-29693.
- Liu, J., Huang, J., Cai, Q., Yang, Y., Luo, W., Zeng, B., Xu, Y., Yuan, C. and Dai, L. (2020). Design of Slidable Polymer Networks: A Rational Strategy to Stretchable, Rapid Self-Healing Hydrogel Electrolytes for Flexible Supercapacitors. *ACS Appl. Mater. Interfaces* 12, 20479-20489.
- Liu, Z., Liang, G., Zhan, Y., Li, H., Wang, Z., Ma, L., Wang, Y., Niu, X. and Zhi, C. (2019). A soft yet device-level dynamically super-tough supercapacitor enabled by an energy-dissipative dual-crosslinked hydrogel electrolyte. *Nano Energy* 58, 732-742.
- Lu, C. and Chen, X. (2020). All-Temperature Flexible Supercapacitors Enabled by Antifreezing and Thermally Stable Hydrogel Electrolyte. *Nano Lett.* 20, 1907-1914.
- Lu, N., Na, R., Li, L., Zhang, C., Chen, Z., Zhang, S., Luan, J. and Wang, G. (2020). Rational Design of Antifreezing Organohydrogel Electrolytes for Flexible Supercapacitors. *ACS Appl. Energy Mater.* 3, 1944-1951.
- Peng, H., Lv, Y., Wei, G., Zhou, J., Gao, X., Sun, K., Ma, G. and Lei, Z. (2019). A flexible and self-healing hydrogel electrolyte for smart supercapacitor. *J. Power Sources* 431, 210-219.
- Sun, K., Feng, E., Zhao, G., Peng, H., Wei, G., Lv, Y. and Ma, G. (2019). A Single Robust Hydrogel Film Based Integrated Flexible Supercapacitor. *ACS Sustainable Chem. Eng.* 7, 165-173.
- Tang, Q., Chen, M., Wang, G., Bao, H. and Saha, P. (2015). A facile prestrain-stick-release assembly of stretchable supercapacitors based on highly stretchable and sticky hydrogel electrolyte. *J. Power Sources* 284, 400-408.
- Tang, Q., Chen, M., Yang, C., Wang, W., Bao, H. and Wang, G. (2015). Enhancing the Energy Density of Asymmetric Stretchable Supercapacitor Based on Wrinkled CNT@MnO<sub>2</sub> Cathode and CNT@polypyrrole Anode. *ACS Appl. Mater. Interfaces* 7, 15303-15313.
- Wang, J., Liu, F., Tao, F. and Pan, Q. (2017). Rationally Designed Self-Healing Hydrogel Electrolyte toward a Smart and Sustainable Supercapacitor. *ACS Appl. Mater. Interfaces* 9, 27745-27753.
- Wang, Z., Tao, F. and Pan, Q. (2016). A self-healable polyvinyl alcohol-based hydrogel electrolyte for smart electrochemical capacitors. *J. Mater. Chem. A* 4, 17732-17739.
- Wei, J., Zhou, J., Su, S., Jiang, J., Feng, J. and Wang, Q. (2018). Water-Deactivated Polyelectrolyte Hydrogel Electrolytes for Flexible High-Voltage Supercapacitors. *ChemSusChem* 11, 3410-3415.
- Ye, T., Li, D., Liu, H., She, X., Xia, Y., Zhang, S., Zhang, H. and Yang, D. (2018). Seaweed Biomass-Derived Flame-Retardant Gel Electrolyte Membrane for Safe Solid-State Supercapacitors. *Macromolecules* 51, 9360-9367.
- Zhao, J., Chen, Y., Yao, Y., Tong, Z., Li, P., Yang, Z. and Jin, S. (2018). Preparation of the polyelectrolyte complex

hydrogel of biopolymers via a semi-dissolution acidification sol-gel transition method and its application in solid-state supercapacitors. *J. Power Sources* 378, 603-609.

Zhou, Y., Wan, C., Yang, Y., Yang, H., Wang, S., Dai, Z., Ji, K., Jiang, H., Chen, X. and Long, Y. (2019). Highly Stretchable, Elastic, and Ionic Conductive Hydrogel for Artificial Soft Electronics. *Adv. Funct. Mater.* 29, 1806220.